THE THEORY AND MATHEMATICAL DEVELOPMENT OF AIRPOL-4

by

William A. Carpenter
Research Engineer

and

Gerardo G. Clemeña
Research Analyst

(The opinions, findings, and conclusions expressed in this report are those of the authors and not necessarily those of the sponsoring agencies.)

ABSTRACT

This is the first in a series of reports documenting the Virginia Department of Highways & Transportation line source model for predicting carbon monoxide concentrations within the microscale environments of highways. The purpose of this first report is to provide a detailed introduction to and verification of the theoretical development of AIRPOL-4, a true Gaussian formulation enhanced by several theoretical and computational innovations.

These innovations establish AIRPOL-4 as a major advancement in the field of air quality modeling. Specifically, the mathematical development of the conceptual aspect of the model demonstrates AIRPOL-4's ability to correctly analyze

      1. receptors upwind of a roadway,
      2. all wind speeds ≥ 0,
      3. any sampling interval,
      4. urban environments,
      5. all traffic speeds ≥ 0, and
      6. at grade, cut, and fill geometries.

Furthermore, the algorithmic development of the model firmly establishes AIRPOL-4's position as a very efficient and very accurate model.

The second report in this series provides the definitive experimental evidence of AIRPOL-4's prepotent predictive performance and cost effectiveness.

TABLE OF CONTENTS

v

3006

LIST OF FIGURES

ACKNOWLEDGEMENTS

THE THEORY AND MATHEMATICAL DEVELOPMENT OF AIRPOL-4

by

William A. Carpenter
Research Engineer

and

Gerardo G. Clemeña
Research Analyst

INTRODUCTION

Motor vehicles are a major source of carbon monoxide (CO) pollution. Consequently, CO concentrations are often highest in the vicinity of highways. Because of the potential health hazard that CO from future highway developments pose, it is desirable to have a reliable means of estimating expected CO concentrations near proposed highways for any combination of traffic and meteorological conditions.

At present, there are several mathematical models available for estimating CO concentrations in the vicinity of a highway. Based on their approach, these models can be classified into two general groups: those that use the mass-conservation equation (K theory),[1, 2]

$$U \frac{\partial C}{\partial x} = K_y \frac{\partial^2 C}{\partial y^2} + K_z \frac{\partial^2 C}{\partial z^2} \tag{1}$$

and those that use various modifications of the basic Pasquill-Gifford Gaussian plume equation for point sources, which is a special case solution of the mass-conservation equation,[3, 4, 5, 6, 7, 8, 9, 10]

$$C = \frac{Q}{2\pi\mu} * \left\{ \frac{e^{\left[-\frac{1}{2}\left(\frac{y}{\sigma_y}\right)^2\right]}}{\sigma_y} * \frac{e^{\left[-\frac{1}{2}\left(\frac{z-h}{\sigma_z}\right)^2\right]} + e^{\left[-\frac{1}{2}\left(\frac{z+h}{\sigma_z}\right)^2\right]}}{\sigma_z} \right\} \tag{2}$$

where C is the pollutant concentration;

μ is the mean wind speed in the x direction;

x, y and z are Cartesian axes;

K_y and K_z are the eddy diffusion coefficients in the y and z directions;

Q is the pollutant emission rate;

σ_y and σ_z are the standard deviations of the distribution of plume concentration in the horizontal and vertical directions; and

h is the effective source height.

Of these two approaches, the first has much greater theoretical versatility. It can take into account complicated cases such as complex topography and horizontal and vertical differences in meteorological variables. However, it requires much greater computing time, and input data that are, in practice, indeterminant. On the other hand, the Gaussian approach is simpler, easier to apply, and the input data required are readily available. Thus in practice, the Gaussian approach is the most widely used.

Although the Gaussian formulation for a point source, equation 2, can readily be extended to a line-source formulation by integration over the line source, the resulting integral equation has no analytic solution. [11] As a result, the designers of many so-called Gaussian models have employed gross simplifications and assumptions to reduce the integral to an analytic equation, which has resulted in operative but hardly justifiable models, while others have applied general purpose numerical techniques, a costly and often inaccurate approach, in the search for a solution to the integral form of the Gaussian formulation. These and other difficulties with available Gaussian models persuaded the Virginia Highway & Transportation Research Council to develop AIRPOL-4, a cost effective and versatile Gaussian formulation. [12, 13, 14] This report details the concept and mathematical development of that model.

THE GAUSSIAN FORMULATION

This section of the report develops the basic geometry and calculus necessary to express CO concentrations at a receptor, either upwind or downwind of a uniform continuous line source, using a Gaussian formulation. The discussion assumes an understanding of the basic Gaussian formulation.

Consider the Euclidean coordinate system shown in Figure 1. It consists of the three perpendicular axes, P, DIST, and Z, aligned such that the DIST axis is parallel to the wind direction vector and the Z axis is perpendicular to the earth. In this system, positive DIST is measured upwind and positive Z is measured upward from the surface of the earth. Within the framework of this system, equation 1 implies that for a point source located at (p, dist, h), and a receptor located at (0, 0, z), the CO concentration at the receptor is

$$C = \begin{cases} \dfrac{Q}{2\pi\mu} * \left\{ \dfrac{e^{\left[-\frac{1}{2}\left(\frac{p}{\sigma_p}\right)^2\right]}}{\sigma_p} * \dfrac{e^{\left[-\frac{1}{2}\left(\frac{z-h}{\sigma_z}\right)^2\right]} + e^{\left[-\frac{1}{2}\left(\frac{z+h}{\sigma_z}\right)^2\right]}}{\sigma_z} \right\} & , \text{ for dist} \geq 0 \\ \\ 0, \text{ for dist} < 0 \end{cases} \tag{3}$$

where:

Q is the source CO emission rate,
μ is the mean wind speed, and
σ_p, σ_z are functions of dist and atmospheric stability.

Now consider Figure 2. Here there are two Euclidean coordinate systems, a roadway, assumed to be a uniform, continuous line source, a receptor, and a wind direction vector. The receptor coordinate system, or the P, DIST, Z system, is the same as that in Figure 1. Within this system the receptor coordinates are (0, 0, z)$_{receptor}$. The roadway coordinate system, or the D, R, H system, is oriented such that the R axis coincides with the roadway, the positive H axis emanates from the earth's surface, positive D is measured on the downwind side of the roadway, and the receptor lies in the DH plane. The observer location relative to this system is (d, 0, z)$_{roadway}$.

Given this information and α, the acute angle between the roadway and the wind vector, it can easily be determined that the roadway coordinate system may be mapped into the receptor coordinate system by a transformation T: (0, r, h)$_{roadway} \longrightarrow$ (p, dist, z)$_{receptor}$. The mathematical form of this transformation is defined by:

$$p = -d * \cos \alpha + r * \sin \alpha, \tag{4}$$

$$dist = d * \sin \alpha + r * \cos \alpha, \text{ and} \tag{5}$$

$$z = h \tag{6}$$

The advantage of using these two coordinate systems and this transformation is that they permit equation 3 to be directly applied to each roadway point to determine the contribution of that point to the pollution at the receptor. The total pollution at the receptor may then be found by integrating equation 3 over all roadway points having nonnegative DIST coordinates in the receptor coordinate system.

Assuming that the road is nearly parallel to the surface of the earth so that h will be nearly constant, this integration may be expressed as

$$C = \frac{Q_L}{2\pi\mu} \int_M^{ULENGH} \left\{ \frac{e^{\left[-\frac{1}{2}\left(\frac{p}{\sigma_p}\right)^2\right]}}{\sigma_p} * \frac{e^{\left[-\frac{1}{2}\left(\frac{z-h}{\sigma_z}\right)^2\right]} + e^{\left[-\frac{1}{2}\left(\frac{z+h}{\sigma_z}\right)^2\right]}}{\sigma_z} \right\} dr \qquad (7)$$

where Q_L is the uniform line source emission rate.

The upper bound of integration, ULENGH, is specified by simple definition, i.e., the distance the roadway extends, in a nearly straight line, upwind from the point $(0, 0, h)_{roadway}$. The lower bound, M, is found by first determining M', the distance between $(0, 0, h)_{roadway}$ and $(0, -d * \tan (\alpha), h)_{roadway}$, the intersection of the R and P axes. The latter point is the natural lower bound of integration since, as equation 5 demonstrates, it is the greatest lower bound of all roadway points having nonnegative DIST coordinates in the receptor coordinate system. However, the possibility that this point will lie farther along the R axis than the road actually extends must be accounted for. Notice that since the receptor is downwind of the road, which implies $d \geq 0$, and since $0° \leq \alpha \leq 90°$, equation 5 requires that $M' \leq 0$. Therefore M must be defined as M = max (M', -DLENGH), where DLENGH is the distance the roadway extends in a nearly straight line downwind from the point $(0, 0, h)_{roadway}$. Thus if equation 7 can be solved, the pollution level at a receptor on the downwind side of a roadway can be predicted.

Now the discussion is extended to include a receptor on the upwind side of a roadway. Figure 3 illustrates a receptor upwind of a roadway source. By the same geometric arguments as were employed for the downwind observer case, it can be seen that equations 4, 5, and 6 again define the mapping of the roadway coordinate system into the receptor coordinate system. Thus equation 3 may again be used to determine the contribution of any roadway point to the total pollution at the receptor, which implies that equation 7 again determines the total pollution at an upwind receptor when the bounds of integration are chosen so as to include only those roadway points having nonnegative DIST coordinates in the receptor coordinate system.

ULENGH, the upper bound of integration, is determined as it was in the downwind receptor case, by simple specification. The point $(0, -d * \tan (\alpha), h)_{roadway}$, the intersection of the R and P axes, is again shown by equation 5 to be the greatest lower bound of all roadway points

- 4 -

having nonnegative DIST coordinates in the receptor coordinate system. However, since the receptor is now upwind of the road, which implies $d \leq 0$, equation 5 shows that M', the distance from $(0, 0, h)_{roadway}$ to $(0, -d * \tan(\alpha), h)_{roadway}$, must be $M' \geq 0$. Therefore, M for an upwind receptor must be defined as M = min (M', ULENGH).

Consideration of the upwind formulation versus the downwind formulation reveals that for the same absolute roadway to receptor distance, $|d|$, $M_U \geq M_D$. Also for any roadway point contained in both intervals, $p_U^2 \geq p_D^2$ and $dist_U \leq dist_D$. Only when $\alpha = 0^o$ does $M_U = M_D$, $p_U^2 = p_D^2$, and

$dist_U = dist_D$, which is reassuring since the upwind and downwind sides of a roadway should be indistinguishable at $\alpha = 0^o$.

In this section it has been shown that there exists a single Gaussian formulation capable of expressing CO concentrations at receptor points either upwind or downwind from a uniform continuous line source. The next section will describe a simple and inexpensive technique for evaluating that formulation.
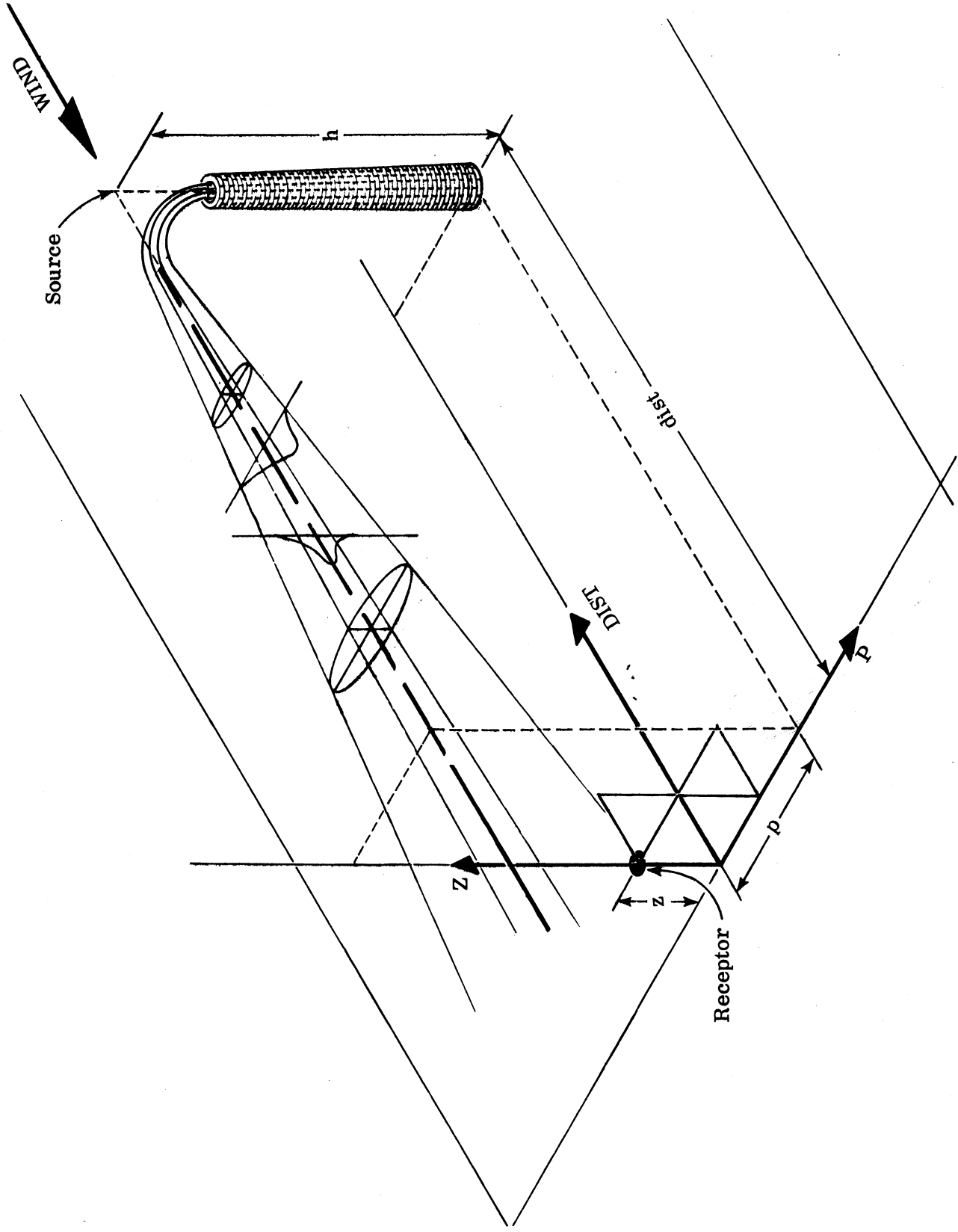
Figure 1. Euclidean coordinate system showing Gaussian distribution in the horizontal and vertical.

CASE = Downwind

$$p = -d * \cos(\alpha) + r * \sin(\alpha)$$

$$dist = d * \sin(\alpha) + r * \cos(\alpha)$$

$$CO(RECEPTOR) = \int_{M}^{ULENGH} CO(d\,ROAD)$$
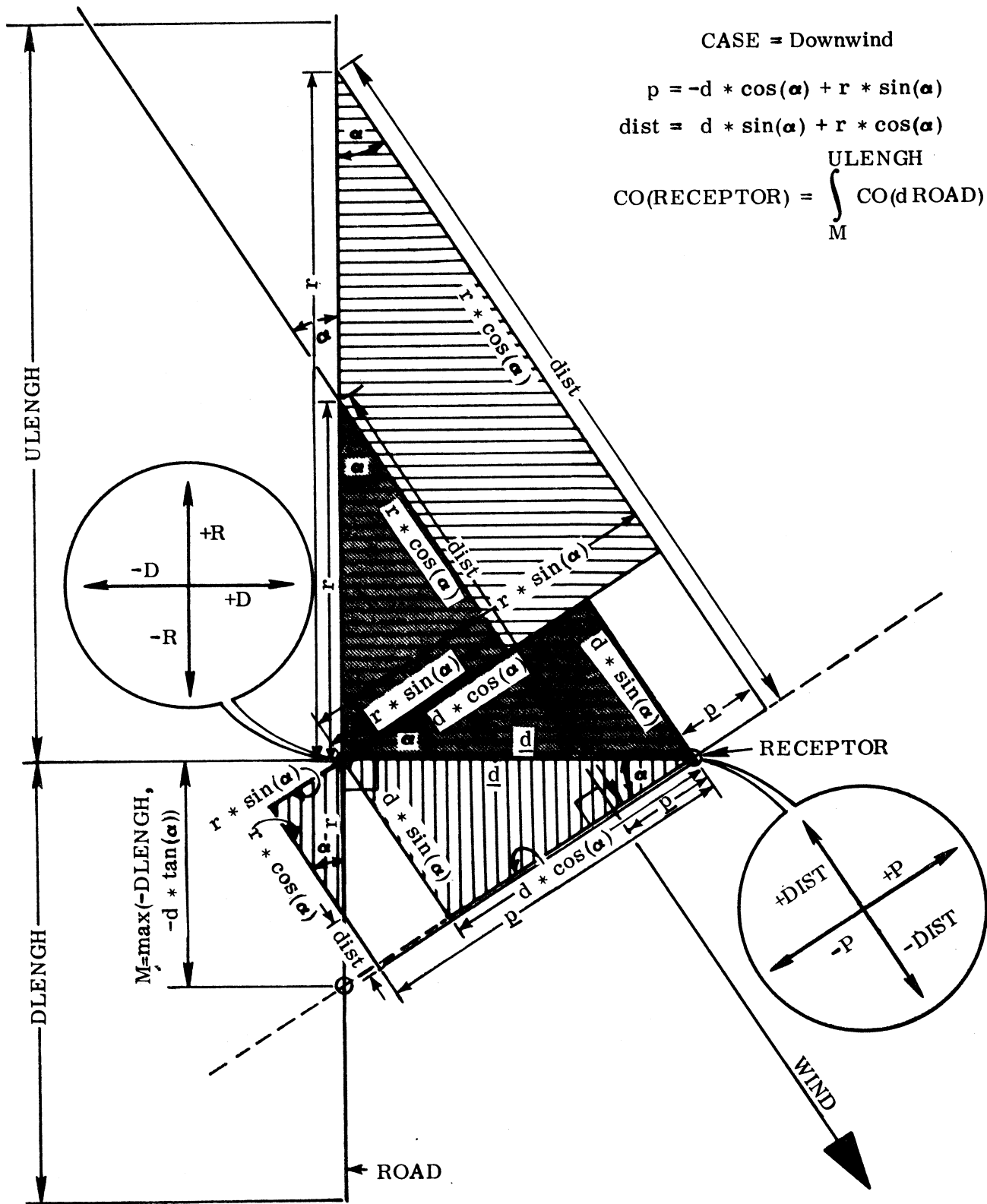
Figure 2. Geometric treatment for downwind receptor.

CASE = Upwind

$$p = -d * \cos(\alpha) + r * \sin(\alpha)$$

$$dist = d * \sin(\alpha) + r * \cos(\alpha)$$

$$CO(RECEPTOR) = \int_{M}^{ULENGH} CO(d\,ROAD)$$

ULENGH

M=min(ULENGH, -d * tan(α))

dist

r * cos(α)

r

r * sin(α)

p

d * cos(α)

d * sin(α)

d

α

RECEPTOR

+DIST

-P   +P

-DIST

+R

-D.   +D

-R

WIND

DLENGH

ROAD

Figure 3. Geometric treatment for upwind receptor.

EVALUATING THE GAUSSIAN LINE SOURCE FORMULATION

As noted earlier, equation 7 has no analytical solution,[11] and numerical integration generally requires a great deal of expense. However, this section will demonstrate an inexpensive mathematical technique capable of evaluating equation 7 accurately.

An examination of the integrand in equation 7 reveals that in the neighborhood $\alpha \approx 90^{\circ}$, it behaves much like

$$g(r) = ae^{-(ar)^2} \tag{8}$$

which implies that in this range, it and its even derivatives reach their extremes in a neighborhood of $r \approx p \approx 0$, and that they decay exponentially away from $p \approx 0$. It can also be noted that in the neighborhood $\alpha \approx 0^{\circ}$, the integrand behaves much like

$$h(r) = \frac{e^{-(\frac{a}{r})^2}}{r} \tag{9}$$

which implies that it and its even derivatives reach their extremes at $r = \lambda \geq 0$.

Further analysis of the integrand demonstrates that these properties extend to a simple characterization of the integrand over the entire ranges of α and d. In particular it can be observed that even though the integrand may not reach its maximum at $p = 0$ for all α, it at least does so in a neighborhood of $p = 0$, whenever this neighborhood exists. Furthermore, in this neighborhood, its derivatives may be estimated within two orders of magnitude by those of equation 8. Also it can be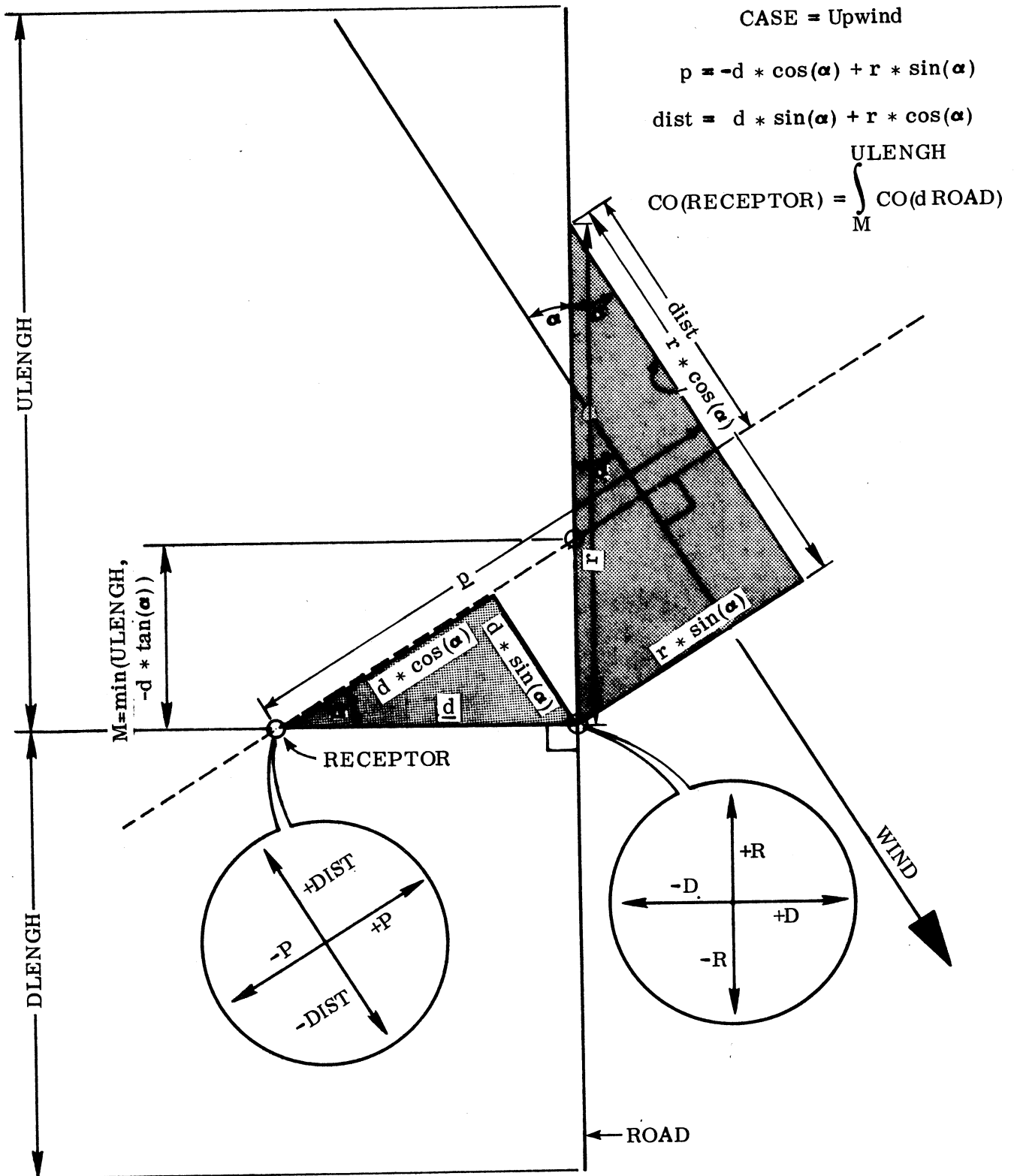 observed that when the $p = 0$ neighborhood does not exist, i.e., in the upwind observer and $\alpha \approx 0^{\circ}$ cases, the integrand and its derivatives reach their maximums in a neighborhood of $r = M$. Furthermore, in this neighborhood, the integrand's derivatives are estimable within two orders of magnitude by those of equation 9. Finally it can be observed that the integrand's derivatives decay rapidly away from either of these neighborhoods.

These observations constitute a characterization, although not a detailed one, of the integrand in equation 7. This lack of detail, however, presents no real problem. Even though a perfect characterization of the integrand is not available, it is known in which two neighborhoods it will be particularly troublesome to evaluate and that outside these neighborhoods it will be relatively easy to evaluate. Thus the application of expensive techniques to easily evaluated intervals, a primary impediment to efficient numerical integration, can be avoided by employing a specialized segmentation technique over the range of integration in conjunction with an appropriate numerical method.

The particular numerical technique selected was the Cote's method of order six, C6, which is in effect a sixth order polynomial approximation of an integrand over a given interval, having an error term of

$$\epsilon = 6.4 * 10^{-10} * (b-a)^9 * f^8(\lambda) \text{ for } \lambda \epsilon (a,b) \tag{10}$$

where $f(\cdot)$ is the integrand, $f^8(\cdot)$ is its eighth derivative, and (a, b) is the interval of integration.[15] C6 was selected in preference to other techniques because of its ability to yield acceptable errors for the fewest number of calculations for equation 7 when used in conjunction with the segmentation technique described below.

The most difficult intervals to integrate numerically are those containing extreme points and large higher order derivatives, while the simplest are those over which the integrand's derivatives approach zero. Therefore, the most fruitful segmentation techniques for equation 7 are those which produce concentrations of interpolation points in the $p \approx 0$ and $r \approx M$ neighborhoods. The specific technique used in AIRPOL-4 is to divide the total interval of integration into twelve subintervals, two each of length 1 meter covering the interval from M to M + 2 and ten covering the remaining range of integration with five on either side of the point p = 0. When the point p = 0 is not an element of (a, b), these ten are split with five on either side of the midpoint of (a, b). The lengths of these ten subintervals increase away from the point p = 0, or the midpoint, in the ratio of 1:2:3:5:10, under the restriction that the first four on either side have maximum lengths of 10, 20, 30, and 50 meters while the last one on either side is unconstrained. The number, lengths, and locations of these subintervals were determined from the criterion that the maximum integration error should result in no more than approximately ±0.02 ppm CO prediction error for a superposition of three line sources, which translates to an error of approximately ±0.007 meters for the integral in equation 7, or approximately $±6 * 10^{-4}$ meters for each subinterval.

In defining this segmentation technique, $f^8(\cdot)$ in equation (10) was estimated as

$$f^8(\cdot) \approx \max\left(\left| g^8(\cdot) \right|, \left| h^8(\cdot) \right| \right) \tag{11}$$

which is approximately

$$f^8(\cdot) \approx \max\left(\left| 256 * e^{\left(-\frac{p^2}{a}\right)} * \frac{p^8}{a^{17}} \right|, \left| 256 * e^{\left(-\frac{a^2}{r}\right)} * \frac{a^{16}}{r^{24}} \right| \right) \tag{12}$$

where $a \approx (\sigma_y + \sigma_z)$.

With this approximation for $f^8(\cdot)$ the above defined subintervals provided the necessary integration accuracy with a minimum safety factor of about two orders of magnitude which, given the uncertainty of $f^8(\cdot)$, was considered acceptable.

In summary, to obtain an error bound of ± 0.02 ppm CO for a superposition of three lane groups, the technique employed by AIRPOL-4 requires the calculation of only 72 data points from the line source. Any polynomial type integral approximation which uses fixed interval lengths would in the general case require approximately six data points per meter of line source to achieve this same accuracy. Thus, for a roadway length of about two kilometers the AIRPOL-4 technique would be on the order of 200 times more efficient than a fixed interval technique yielding the same accuracy. Furthermore, compared to progressive fixed interval techniques, such as the Simpson's Rule with successive bisection, which has the potential to completely miss the extreme point/high derivative subinterval before termination, this specialized segmentation technique with C6 is potentially more accurate as well as more efficient.

With the basic model to be used and the numerical technique for evaluating that model established, consideration is next given to the details necessary to complete the model. The next section examines the problems of determining stability class and evaluating the dispersion parameters σ_y and σ_z.

ATMOSPHERIC STABILITY AND THE GAUSSIAN
DISPERSION PARAMETERS

Gaussian dispersion theory is based on the premise that pollutants are distributed normally in the vertical and horizontal directions about the center-line of the plume from a point source. Thus the proper determination of σ_y and σ_z, the standard deviations of dispersion in the horizontal and vertical directions, is central to any effective implementation of the Gaussian theory.

The first step in evaluating these dispersion parameters is to determine the prevailing atmospheric stability class for the time period of interest. Two simple techniques for determining stability class, Turner's method[16] and a slightly modified Pasquill method[17], were evaluated for use with AIRPOL-4. The Pasquill method was found to be substantially superior to the Turner method. A third method, that of directly measuring the variability of wind flows in the vertical and horizontal directions, would actually be the most effective technique; however, it cannot be used in normal applications of the model since such wind data are not typically available. Thus, AIRPOL-4 is designed to perform using Pasquill stability estimates on the strength of their superior performance and the availability of data for typical predictive applications.

However, it must be emphasized that the model's performance is limited by the inability of either Pasquill's or Turner's method to yield values of the dispersion parameters in good agreement with measured wind variabilities. This is a problem common to all Gaussian models and would thus be a fruitful area in which to conduct further research to improve the performance of this class of models.

The second step in determining the dispersion parameters is to establish the functional form of σ_y (CLASS, DIST) and σ_z (CLASS, DIST). Turner, in reference 5, presents Pasquill's graphs of σ_y and σ_z for stability classes A through F and plume centerline distances from 0.10 to 100 kilometers. However, a major area of interest when predicting highway generated air pollution is the first 100 meters from the roadway. Thus some method of extrapolating Pasquill's curves must be found.

AIRPOL-4 incorporates the method employed by Zimmerman and Thompson in the HIWAY model.[8] The essence of this technique is the extrapolation of the σ_y, σ_z curves to the values $\sigma_y = 3.0$ meters and $\sigma_z = 1.5$ meters. This extrapolation determines the distances at which these σ_y, σ_z values were achieved for each stability class. These distances may then be used as offset parameters in the functional expressions for σ_y and σ_z. This method thus yields final functional forms of σ_y (CLASS, DIST + OFFSET$_{CLASS}$), and σ_z (CLASS, DIST + OFFSET$_{CLASS}$), which have been found to perform reliably in AIRPOL-4.

Although this technique is basically reliable and should provide conservative CO estimates, [8, 14] one must be cognizant of the fact that it is nothing more than an extrapolation of Pasquill's empirical data down to the exiguous EPA data indicating $\sigma_y \approx 3.0$ meters and $\sigma_z \approx 1.5$ meters at the edge of the mechanical mixing cell. Furthermore, the technique is nondeterministic as evidenced by the fact that the σ_y and σ_z values in HIWAY and AIRPOL-4 are not the same. This apparent anomaly results from the employment of extrapolation and curve fitting techniques of differing precision.

Thus it is seen that σ_y and σ_z are at best only estimates of the true dispersion parameters when the Gaussian assumption of no localized eddy effects is met. This problem is common to all Gaussian models and should receive serious research consideration. It is unlikely that there will be any more major advancements in Gaussian pollution modeling until a more reliable method of determining dispersion parameters is found.

Another problem of Gaussian modeling relating to the determination of σ_y and σ_z is that Pasquill's curves are intended to define dispersion parameters over open rural country for time intervals of 3 to 10 minutes. Typically one wants to apply a model such as AIRPOL-4 to an urban area for time intervals other than 3 to 10 minutes. Fortunately, this problem has a mathematical solution, which is presented in the next section.

DISPERSION PARAMETERS AND SAMPLING TIMES

Prevailing winds vary with time on both macro-and microscales. Over short time intervals macro variation is nearly zero, leaving the micro variation as the primary contributor to σ_y. However, for larger time intervals macro variation has a significant effect on horizontal dispersion. Thus, since the Pasquill curves for σ_y are based on 3 to 10 minute sampling times, they ignore much of the effect of macro wind variations in the horizontal for longer sampling times.

Turner[5, 19] discusses this problem although he never constructs a general case mathematical solution to it. He does, however, provide the insights necessary to develop such a solution. He cites empirical results for constant mean wind direction relating plume centerline concentration to sampling time. These results indicate that for any two sampling times the ratio of the time averaged centerline concentrations will be an inverse power function of the ratio of their sampling times.

Equation 3 reveals that the ratio of two plume centerline concentrations reduces to the inverse ratio of their respective $\sigma_y * \sigma_z$ products. If one assumes, as Turner suggests, that σ_z is nearly constant with time, then the ratio of σ_y values for two different sampling times will be a power function of the ratio of their sampling times (see equation 13) and that all the variation in concentration with sampling time will be attributable to the variation in σ_y.

This deduction now permits the determination of the concentration variation with sampling time for receptor points other than those on plume centerlines and thus for receptors affected by line sources. This determination is accomplished by merely adjusting Pasquill's σ_y values using a power function of the ratio of sampling times and calculating CO concentrations based on the revised values of σ_y. Thus all that remains is to properly define these power functions.

The most interesting approach cited by Turner[19] is one expressing the power law for plume centerline concentrations in terms of atmospheric stability class. Algebraic manipulation to extend this approach to the general case yields

$$\frac{(\sigma_y)_{T_2}}{(\sigma_y)_{T_1}} = \left(\frac{T_2}{T_1}\right)^P \tag{13}$$

where the suggested values are

$$P = 0.65, \text{ for Class A,}$$
$$P = 0.52, \text{ for Classes B \& C, and}$$
$$P = 0.35, \text{ for Class D.}$$

However, this relationship still does not provide the total correspondence with stability class which the present authors felt was necessary. Therefore, interpolations and extrapolations were made using an increasing interval technique to determine the dependence of P on stability class. The resulting values of P are

$$P = 0.65, \text{ for Class A,}$$
$$P = 0.56, \text{ for Class B,}$$
$$P = 0.46, \text{ for Class C,}$$
$$P = 0.35, \text{ for Class D,}$$
$$P = 0.23, \text{ for Class E, and}$$
$$P = 0.10, \text{ for Class F.}$$

This technique can thus be used to convert $(\sigma_y)_{T_1}$ to $(\sigma_y)_{T_2}$, where T_1 is the time base for the given σ_y values and T_2 is the actual required sampling time. However, T_1 is not well-defined. Pasquill's curves are intended for $T_1 = 3$ to 10 minutes, which is too indefinite for use in equation 13. Also it will be recalled that Pasquill's curves are for σ_y and σ_z over open rural countryside whereas highway air pollution predictions are typically required for urban areas and such environments tend to have characteristically higher atmospheric turbulence.

Consideration of equation 13 reveals that increasing T_1 tends to correct Pasquill's curves to those expected for an urban environment. Thus to account for this possibility, values of T_1 from 3 to 60 minutes were empirically examined to determine an optimal value. The resulting optimum was found to be $T_1 = 15.5$ minutes, which, as expected, is larger than Pasquill's 3 to 10 minutes due to the change in environment. Thus this led to a rather simple mathematical technique for enabling AIRPOL-4 to adjust Pasquill's curves from those for rural environments with 3 to 10 minute sampling intervals to those for urban environments with a sampling interval = T_2 minutes where T_2 may be specified by the user.

The reader may be concerned that only σ_y has been adjusted while σ_z has been unaltered. Turner states that variation in the horizontal wind direction is the primary cause of CO variation with sampling time. He does, however, concede that for unstable atmospheric conditions some macro variation in vertical wind direction may occur, but no empirical results are cited. Therefore it is felt that the safest approach would be to ignore macroscale vertical wind variations, because there were no data available and these variations are not the primary cause of CO variation with sampling time.

In the next two sections consideration is given to several refinements of the Gaussian formulation necessary to produce the AIRPOL-4 model.

TREATMENT OF DEPRESSED ROADWAYS

The basic Gaussian formulation is capable of analyzing only those geometric configurations in which both source and observer are at or above ground level. However, other geometries can yield to Gaussian analysis under a proper set of transformations. AIRPOL-4 has been designed to analyze geometries other than the basic at grade configuration. In particular, AIRPOL-4 is capable of analyzing configurations in which a highway is in a cut and an observer is outside the cut. (See Figure 4.) In the steady state, with such a configuration the cut is "full" of gaseous emissions. Thus a mass balance indicates that the amount of CO leaving the top of the cut must equal that generated on the road at the bottom of the cut. Therefore the observer will be cognizant only of a virtual source at the top of the cut. [8,10] This virtual source will not, however, have the same dimensions as would the mechanical mixing cell of an actual source. This circumstance is the result of the dispersion which takes place between the road and the top of the cut.

The shape of the virtual source "mixing cell" can be estimated by assuming first that the principal distortion will occur in the horizontal and that therefore σ_{z_0} will remain approximately 1.5 meters. Secondly it must be realized that due to turbulence in the cut, the "mixing cell" will spread horizontally within an angle of about $0^\circ \leq \beta \leq 90^\circ$ as it rises from the road, if it is unconstrained by the walls of the cut. For a cut of depth CHT meters then σ_y at the top of the cut will be

$$\sigma_{y_0} = 3.0 + 2 * \tan (\beta/2) * CHT, \text{ meters.} \tag{14}$$

Integration over the estimated range of β yields;

$$\sigma_{y_0} \approx 3.0 + 0.88 * CHT, \text{ meters.} \tag{15}$$

If, however, the rising "mixing cell" is constrained from spreading in the horizontal by the walls of the cut CWIDTH meters wide, then σ_{y_0} could never get larger than approximately 3.0 + CWIDTH/6, meters. Therefore, for this geometry the final form of σ_{y_0} becomes

$$\sigma_{y_0} \approx 3.0 + \min (0.88 * CHT, CWIDTH/6.0), \text{ meters.} \tag{16}$$

Thus the only transformations necessary to analyze this source/observer geometry are to locate the virtual source at the top of the cut and to establish σ_{y_0}, which, in turn defines a new offset parameter for the σ_y function. The final outcome of these transformations is then to model this geometry with larger horizontal dispersion parameters and a virtual source at the top of the cut as one intuitively would have surmised.

The analysis of a geometry which places both a roadway and a receptor in a cut is quite difficult under the Gaussian formulation. This geometry generally places the receptor in a field of strong localized eddies, an untenable situation for a gaussian model. However, in the parallel wind case, the effects of localized eddies are minimized as the wind channels down the cut with little disturbance. Thus the Gaussian formulation is an acceptable modeling technique for this geometry, given that the wind flow must be confined to the parallel case.

This conditional application of the Gaussian formulation is not as restrictive as it might at first appear. Surface winds in general tend to channel down a cut section. Furthermore, when wind flows are not parallel to a cut section, they tend to produce a higher turbulence in the cut. Thus modeling the parallel wind condition in a cut section should produce at least an order of magnitude estimate of, and will often produce an upper bound for, the general case condition.

There are two transformations necessary to analyze this restricted version of a road and a receptor in a cut. First, one must determine the distance, X, beyond the mouth of the cut from which significant amounts of pollutant will enter the cut and thus contribute to the pollutant level at the receptor. This may be accomplished by finding X, in meters, such that

$$\sigma_y (X) = 4 * CWIDTH, \tag{17}$$

where CWIDTH is the cut width in meters. Equation 17 produces a conservative estimate of X since only about 70% of the pollutants from points less than X meters from the mouth of the cut will enter the cut, while virtually none of the pollutants from points greater than X will enter. To further assure a conservative estimate, stability class F is used to solve for X, and gives

$$4 * CWIDTH = \sigma_y (X) = 0.06387 * (X + 72.0415)^{0.9000} \tag{18}$$

which yields

$$X = \left(\frac{4 * CWIDTH}{0.06387}\right)^{1.1111} - 72.0415 \text{ meters.} \tag{19}$$

This value of X is then used to determine ULENGH, the upper limit of integration by taking

$$ULENGH = \min (ULENGH, CLENGH + X), \text{ in meters.} \tag{20}$$

The reader should also recall that for parallel winds, the lower limit of integration is M = 0.

The second transformation necessary to analyze this geometric condition is one to account for the horizontal confinement of pollutants by the canyon walls. Vertical dispersion will, of course, be unaffected by the cut. Pollutants from any point on the roadway will disperse downwind in a Gaussian fashion in the horizontal until they reach the cut walls. At this downwind distance,

reflections from the canyon walls will cause their distribution to begin a transition from a normal, N $(0, \sigma_y^2)$, distribution to a uniform, U (-CWIDTH/2 + CWIDTH/2) distribution. This transition will evolve over some downwind distance which will be a function of CWIDTH and σ_y.

Thus depending on their upwind distances from a receptor, roadway points will present either a Gaussian, transition, or uniform distribution of pollutants at the receptor. A receptor in a cut will therefore, in general, perceive pollutants having all three distributions.

In order to generate the transition and uniform distributions from the normal distribution, the form

$$\left[\frac{1}{\sqrt{2\pi}\ \sigma_y} \ * \ e^{-\frac{1}{2}\left(\frac{P}{\sigma_y}\right)^2} \right]$$

is allowed to mutate to the form

$$\left[\frac{1}{CWIDTH} \right]$$

as reflections from the canyon walls increase with increasing travel distance. This transition must therefore commence when σ_y reaches approximately 1/6 to 1/4 of CWIDTH and progress geometrically as the travel distance increases. An elegant yet simple technique for generating this transition distribution and its limiting uniform distribution is to allow σ_y in the denominator of the Gaussian distribution to decay to CWIDTH/2 as DIST increases beyond the point where CWIDTH $\approx 5 \ * \sigma_y$. Thus all three distributions may be mathematically described by the transformation

$$T: \quad \left(\frac{1}{\sqrt{2\pi}\ \sigma_y}\right) \ e^{-\frac{1}{2}\left(\frac{P}{\sigma_y}\right)^2} \ \rightarrow \ \left(\frac{1}{\sqrt{2\pi}\ \sigma_y^*}\right) \ e^{-\frac{1}{2}\left(\frac{P}{\sigma_y}\right)^2} \ ,$$

where

$$\sigma_y^* = \begin{cases} \sigma_y, \ \text{for} \ \ \sigma_y \leq \dfrac{CWIDTH}{2\sqrt{2\pi}} \\[3mm] \dfrac{CWIDTH}{2\sqrt{2\pi}} \left[1 + \exp\left(-1\Big/\left(\sigma_y - \dfrac{CWIDTH}{2\sqrt{2\pi}}\right)\right) \right], \ \text{for} \ \sigma_y > \dfrac{CWIDTH}{2\sqrt{2\pi}} \end{cases} \qquad (21)$$

Thus the road-and-receptor-in-a-cut geometry may be analyzed within the Gaussian framework, assuming only that the parallel wind case is at least an order estimator for the general wind case. Modification of the upper limit of integration and application of the decay function for transition from a normal to a uniform distribution enable the transformation of the basic Gaussian model to a form capable of analyzing this geometric condition.

The next section discusses the transformations necessary to analyze elevated roadways.

Plume

Observer
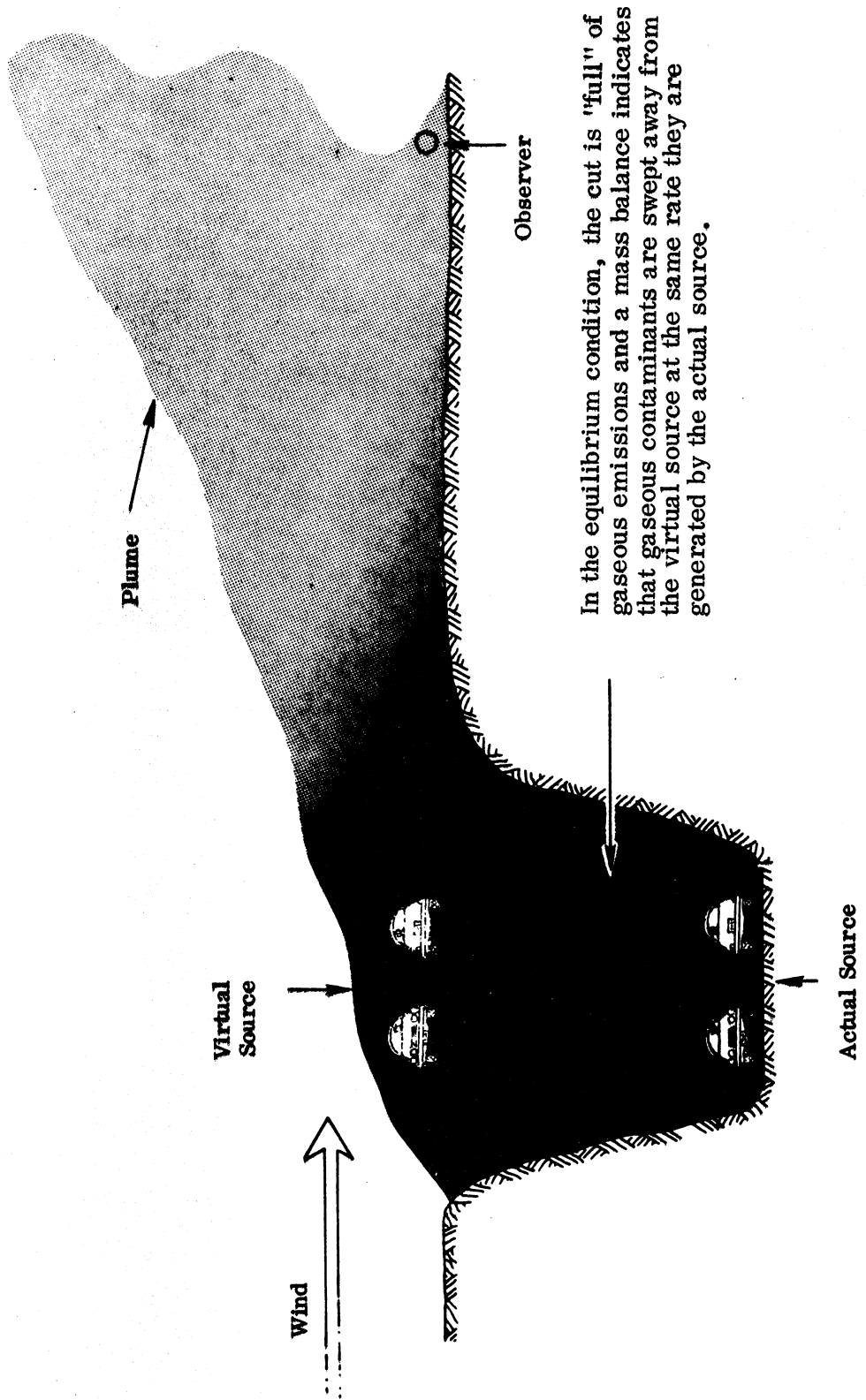
In the equilibrium condition, the cut is "full" of gaseous emissions and a mass balance indicates that gaseous contaminants are swept away from the virtual source at the same rate they are generated by the actual source.

Virtual Source

Actual Source

Wind

Figure 4. Receptor outside a depressed roadway.

- 19 -

TREATMENT OF ELEVATED ROADWAYS

Although the Gaussian formulation is capable of analyzing elevated sources, it is not capable of directly analyzing the air quality effect of a highway fill section. The basic Gaussian "stack" equations assume that a smokestack does not materially obstruct or alter air flow over the surface of the earth. A fill section of highway does, however, drastically alter surface wind flow since it forms a physical barrier over which air must circulate.

Wind flows over highway fills produce vertical turbulence to a height of 1.5 to 2.0 times the height of the barrier[19] and produce strong localized eddy effects in the region of the mechanical mixing cell. Thus a basic Gaussian model cannot yield acceptable results for highway fill geometries. AIRPOL-4, therefore, attempts to transform the basic Gaussian approach to compensate for this shortcoming.

A partial solution to the problem is to transform σ_z to account for the increased vertical turbulence caused by the fill. Since the vertical disturbance extends to 1.5 to 2.0 times HEIGHT, the fill height in meters, the obvious transformation is to increase σ_{z_0} by approximately HEIGHT/4. The implication of this transformation then is that σ_{z_0} is set to

$$\sigma_{z_0} = 1.5 + HEIGHT/4, \text{ meters} \qquad (22)$$

yielding a new

$$ZOFSET = \left[(1.5 + HEIGHT/4)/a\right]^{1/b}, \text{ meters} \qquad (23)$$

where a and b are determined by stability class. This offset is then applied to all σ_z.

This transformation accounts for the increased vertical turbulence produced at the top of a fill by wind shear. It does not, however, account for the fact that wind flow beneath the source is obstructed by the fill. Therefore, this transformation alone is incapable of accounting for the non-Gaussian distribution of pollutants below a fill section.

In fact, then, within the Gaussian framework there is no transformation which is fully capable of accounting for the distribution of pollutants below a fill section. The presence, therefore, of a fill section will cause AIRPOL-4 to underpredict CO concentrations for receptors within approximately $10 * HEIGHT * \sin(\alpha)$ meters of the road. (Field measurements[13, 14] have determined that within this distance from a fill section, AIRPOL-4 will have a probable error of prediction of 1.14 ppm CO.)

Of course, AIRPOL-4 is applicable to the analysis of pollutant distributions from structurally elevated roadways, since bridge type structures permit wind flow below the road surface. The next section develops the technique used in AIRPOL-4 to generate accurate predictions for all positive wind speeds.

THE WIND SPEED DILEMMA

The basic Gaussian dispersion theory is based entirely on the effect of macroscale air movement and its induced eddy effects exclusive of localized eddy and molecular dispersion effects. Therefore, this theory indicates an inverse linear relationship, $CO \propto \frac{1}{\mu}$, between wind speed and pollutant levels when examined in the context of a mass balance. This relationship, however, requires that CO asymptotically approach infinity as μ approaches zero. This situation is, of course, intuitively and empirically unrealistic.

Field data verify that while an inverse linear relationship yields reasonable predictions at high wind speeds (greater than approximately 3 m/s), it produces progressively poorer estimates as wind speeds decrease.[13, 14] The reason for this behavior is that as wind speeds decrease, the dispersion effects of molecular diffusion, vertical thermal transport, and localized mixing replace the decreasing dispersion effects produced by macroscale air movement.

In order to properly model this type of behavior, the authors first proposed a relationship of the form

$$CO \propto \frac{1}{f(\mu, CLASS) + \mu} \qquad (24)$$

where $f(\cdot)$ was to establish the extent to which secondary transport mechanisms affect pollutant dispersion. However, there was not sufficient stability class data available to reliably develop equation 24. The alternative form, which was empirically realizable and which has proven very fruitful,[12] is

$$CO \propto \frac{1}{f(\mu) + \mu} \ . \qquad (25)$$

The relationship in this form incorporates most of the elegance of equation 24, since CLASS is a function of wind speed, yet retains sufficient simplicity to permit empirical justification.

Logical consideration of the problem indicates that the function $f(\cdot)$ in equation 25 must obviously decrease with increasing wind speed. Such consideration also indicates that equation 25 must be finite and have a negative first derivative which decays to zero with increasing wind speed.

Given these constraints, it was decided to consider all variants of the function $(\mu + a * \exp(b * \mu))^{-1}$ since it provided the most versatility in the simplest form. Optimization of this function over 436 data points then produced

$$CO \propto (\mu + 1.92 * \exp(-0.22 * \mu))^{-1}. \qquad (26)$$

The implication of equation 26 is that at very low wind speeds, which the reader will recall are indicative of high atmospheric instability, CO is inversely proportional to 1.92; but as wind speed increases, CO becomes inversely proportional to μ, which is the functional form directly obtained from the Gaussian theory. Equation 26 differs from the pure Gaussian form by 3 db at 1.42 m/s, 6 db at 0.57 m/s, and 9 db at 0.26 m/s.

Thus, although the basic Gaussian formulation produces totally untenable results as wind speeds approach zero, the simple modification characterized by equation 26 enables AIRPOL-4 to produce accurate[14] results over the entire range of feasible wind speeds when the right-hand side of equation 26 is used to replace $1/\mu$ in equation 7.

This section concludes the description of the modifications necessary to upgrade the basic Gaussian formulation to a more accurate and more versatile model, AIRPOL-4. The next section examines the heart of any highway pollution prediction scheme, the estimation of pollution emission rates.

EMISSION FACTORS

Manual determination of CO emission rates is a tedious and error-prone task. Therefore the computer program, AIRPOL-4, contains a sub-program, EFCO (YEAR, MIX, SPEED), which determines average vehicular emission rates given the calendar year, traffic mix, and average traffic speed for the condition in question.

EFCO is based on the methodology proposed by the EPA in reference 20, enhanced by data conventions to improve its computational efficiency and an algebraic transformation to increase its range of applicability. These modifications, which do not, of course, violate the guidelines detailed in reference 20, are discussed below.

For the sake of computational efficiency and the sanity of the user, EFCO considers only two classes of motor vehicles — passenger vehicles and heavy duty vehicles. To further simplify the calculations while providing an upper bound for average CO emission rates, all passenger vehicles are treated as gasoline powered cars and all heavy duty vehicles are treated as gasoline powered trucks.

A major enhancement of the basic EPA algorithm contained in EFCO is the employment of a simple algebraic identity which makes EFCO esthetically and computationally more viable than the EPA procedure. The basic EPA method determines an emission rate in gm/veh/km for an average vehicle speed of 31.5 km/hr and uses a dimensionless speed correction factor, f (S), see Figure 3.1.1-1 ref. 20, to convert this emission rate to a rate for S km/hr, i.e.

$$ER_s = ER_{31.5} * f\ (S).\qquad(27)$$

This emission rate is then multiplied by the traffic volume, V, vehicles per hour to yield the line source emission strength, in gm/km/hr, i.e.,

$$LSER_s = ER_s * V.\qquad(28)$$

The difficulty here is that f (S) approaches infinity asymtotically as S approaches zero, while V approaches zero as S does. Therefore, one is faced with the computationally error-prone prospect of calculating the product of a very large number and a very small number at low traffic speeds. Furthermore, equation 28 becomes indeterminate at S = 0. The problem is further compounded by the fact that no functional form for f (·) is given in reference 20 and the curve of f (·), Figure 3.1.1-1, reference 20, does not even extend below 20 km/hr. Therefore, since equations having indeterminate forms should never be used to model real world events and since extrapolation of asymptotically increasing functions is certainly inadvisable, AIRPOL-4 makes use of the simple identity

$$V = M * S,\qquad(29)$$

where M is the number of vehicles per km. This identity, together with equations 27 and 28, yields

$$LSER_s = ER_{31.5} * f (S) * S * M, \text{ or} \qquad (30)$$

$$LSER_s = ER_{31.5} * f^*(S) * M, \qquad (31)$$

where $f^*(\cdot) = f (S) * S$.

This new speed correction function $f^*(\cdot)$ is a linear function of S. Thus it is very easy to evaluate using the data in Figure 3.1.1-1, reference 20, and its linearity in S eliminates all the difficulties inherent in $f (\cdot)$. The defining equation for $f^*(\cdot)$ is

$$f^* (S) = 28.9639 + S/10 \text{ km/hr.} \qquad (32)$$

The ultimate beauty in using $f^*(\cdot)$ is that at very low, even zero, traffic speeds it is finite. Thus at low speeds, where M can easily be measured, equation 31 provides a computationally viable method of determining $LSER_s$.

The reader should note that the EFCO and EPA techniques are mathematically identical and therefore yield identical results over their computable ranges. The difference in the methods is that the EFCO algorithm has a larger computational range.

There is, however, some risk in using the approach at very low traffic speeds because of the manner in which the EPA has chosen to collect its data. Yet the approach is mathematically viable and must therefore be accepted as the present best estimator given the quality of available data.

EFCO deviates from the EPA's recommended procedure in only one minor respect; i.e., the subprogram uses national average vehicle data where the authors have determined that Virginia -specific data are either inapplicable or unavailable. This deviation and the data base for EFCO are discussed below.

The age distribution of passenger vehicles used in AIRPOL-4 was obtained from Virginia data. The heavy duty vehicle-age distribution, however, was obtained from reference 20, on the assumption that the age distribution of the trucks on Virginia's highways is largely influenced by interstate traffic. EFCO also relies on the national averages cited in reference 20 for annual vehicle miles traveled as a function of vehicle age since such data for Virginia registered vehicles are unobtainable.

SENSITIVITY ANALYSIS

This sensitivity analysis has been divided into five major categories, interaction of variables, sensitivity to meteorological variables, sensitivity to source emission rate variables, sensitivity to geometric variables, and sensitivity to sampling time. Throughout this analysis, all figures, except where noted, have been generated using a two-lane roadway having uniform traffic and geometry with

Average Traffic Mix	=	10% HDV,
Average Traffic Speed	=	90 km/hr,
Downwind Source Length	=	2 km,
Prediction Year	=	1976,
Receptor Height	=	1.5 m,
Road/Wind Angle	=	30°,
Sampling Interval	=	60 minutes,
Source Height	=	0.0 m,
Stability Class	=	D,
Total Traffic Volume	=	2000 veh/hr,
Upwind Source Length	=	2 km, and
Wind Speed	=	2 m/s.

Interaction of Variables

This section discusses the mathematical dependence, independence, and interdependence of the parameters constituting a general Gaussian formulation. Equation 7, which defines the Gaussian line source formulation, may be factored as ·

$$CO = \frac{C_1}{2\pi} * f\,(\cdot) * g_1(\cdot) * g_2(\cdot) * g_3(\cdot) * h(\cdot). \tag{33}$$

The function $f\,(\cdot)$ is the dispersion function resulting from linear transport of pollutants. Thus,

$$f\,(\cdot) = f\ (\text{wind speed}). \tag{34}$$

The functions $g_1(\cdot)$, $g_2(\cdot)$, and $g_3(\cdot)$ are the source emission functions. Thus, $g\,(\cdot)$ describes the line source pollutant emission rate as

$$g\,(\cdot) = g_1\ (\text{traffic volume}) * g_2\ (\text{traffic speed}) * g_3\ (\text{traffic mix, year}). \tag{35}$$

The function $h(\cdot)$ describes the integral of the probablistic dispersion of pollutants from the plume centerlines of an infinite number of point sources. Thus,

$$h(\cdot) = h\ (\text{sampling time, class, wind angle, geometry}). \tag{36}$$

Each of the functions in equation 33 is itself unfactorable. Thus equations 33, 34, 35, and 36 establish the degree of interdependence among the variables constituting a Gaussian formulation.

The sensitivity of CO pollution levels to changes in each of the factors in equation 33 is, of course, a linear function in each of these factors and is independent of each of the other factors. Thus, for those factors which are functions of a single variable, the response of CO levels to changes in that variable is independent of all other variables. Conversely, for those factors which are functions of more than one variable, the responses of CO levels to changes in each of those variables are mutually interdependent on the remaining variables of that function yet are independent of all other variables. Variables of the first kind are thus called "independent", and variables of the second kind are called "interdependent". Wind speed, traffic speed, and traffic volume are the only independent variables in the Gaussian formulation, and CO level is, of course, the only dependent variable. The remaining variables comprise two interdependent groups specified by the factors $g_3(\cdot)$ and $h(\cdot)$. Thus, in the remaining sections of this analysis, the dependencies of CO levels on the parameters of $g_3(\cdot)$ and $h(\cdot)$ have each been necessarily characterized as functions of their respective groups of interdependent variables. The reader should review equations 7 through 23 to gain further insights into this interactive behavior.

Sensitivity to Meteorological Parameters

AIRPOL-4 considers three meteorogical variables, wind speed, wind direction relative to the line source being analyzed, and Pasquill atmospheric stability class each averaged over the user-specified prediction time interval. The characteristic effects of these meteorological variables on CO concentration are illustrated in Figures 5 through 9.

Figure 5 shows the variation in CO concentration profiles with changes in μ, the mean wind speed, meters per second.

Figure 6 demonstrates the actual behavior of $f(\mu)$, equation 34, for both the basic Gaussian model and AIRPOL-4. Since μ is an independent variable, CO concentration varies with μ as $f(\mu)$ does. The reader should particularly observe the asymptotically infinite behavior of

$$f(\mu) = 1/\mu \tag{37}$$

which is used in the basic Gaussian formulation, as contrasted with the finite range of

$$f(\mu) = 1/(\mu + 1.29 * \exp[-0.22 * \mu]), \tag{38}$$

which is used in AIRPOL-4.

As discussed above, field data[13] indicate that equation 37 is generally unacceptable at low wind speeds but produces reasonable predictions above 3 m/s. Notice then, as Figure 6 clearly indicates, that equations 37 and 38 are virtually identical for $\mu > 3$ m/s. Thus the success of equation 38 is a result of its behavior below 3 m/s. This behavior, as discussed previously, is a product of the concept of "residual turbulence", or microscale atmospheric disperson, which arises in the absence of macroscale air movement. This concept demands that equation 34 be rewritten as

$$f(\cdot) = f(\mu, \text{ residual turbulence}) \tag{39}$$

which then yields equation 38 empirically. As a final point, observe that equations 37 and 39 indicate that the basic Gaussian formulation tacitly assumes the residual turbulence to be zero.

Figure 7 illustrates the variation in concentration profiles with changes in atmospheric stability. This variation is, of course, a linear function of $h(\cdot)$, which is itself a function of several mutually interdependent parameters as indicated by equations 33 and 36. (Equations 7 through 23 provide a thorough description of the interaction of these variables.) This figure demonstrates the tendency for concentrations near the source to increase with increasing atmospheric stability, while concentrations far from the source decrease with increasing stability. These changes in concentration profiles are a direct result of the increase in lateral dispersion as atmospheric stability decreases.

Figure 8 is a graph of CO concentration profiles versus α, the acute angle between the road and the mean wind direction. As with stability class, the variation of concentration with angle is a function of the mutually inter-dependent parameters of h (·). The skewing of the characteristic bell-shaped curve toward the downwind receptor and the accompanying decrease in peak concentration as α increases from 0° to 90° is a result of wind action transporting pollutants away from the road rather than down the road. In other words, as α approaches zero (i.e., wind blowing down the roadway) the horizontal crosswind dispersion process becomes important and replaces the downwind dispersion process, as far as concentration levels at a receptor point off the roadway are concerned.

An interesting aspect of Figure 8 is the shape of the $\alpha = 0^o$ curve. This curve, which has the characteristic bell shape, is basically the integral of a sequence of Gaussian curves having increasing variances and constant mean. Thus, in absolute value, the curve has a larger first derivative near the mean and a smaller first derivative far removed from the mean than a pure Gaussian curve. In the $\alpha \neq 0^o$ cases the curves are basically the integrals of sequences of Gaussian curves having non-constant means as well as non-constant variances. However, at small receptor distances from the road, these means do not change appreciably until α nears 90°. Thus, except for the graph at $\alpha = 90^o$, the curves in Figure 8 maintain this characteristicly large first derivative near the roadway.

The function h (·) and its parameters constitute points in a thirteen-dimensional vector space. Thus, to graphically illustrate the total interactive effects of each of these mutually interdependent variables would be infeasible. The interactive impact of CLASS and α as a function of the remaining para-meters of h (·) does, however, deserve comment.

Figure 9 shows the interactive effects of CLASS and α on CO concentrations at receptors 15 meters from the downwind and upwind sides of the roadway. Notice that on the downwind side the peak concentration point shifts from about 3° for stability class F to about 45° for class A. This is a direct result of the interaction of decreasing lateral dispersion with increasing atmospheric stability, and decreasing interval of integration, equation 7, with decreasing α. On the upwind side of the roadway, however, the peak concentration point as a function of α is at $\alpha = 0^o$ for all stability classes. This is the result of the decreasing interval of integration with increasing α on the upwind side of the roadway.
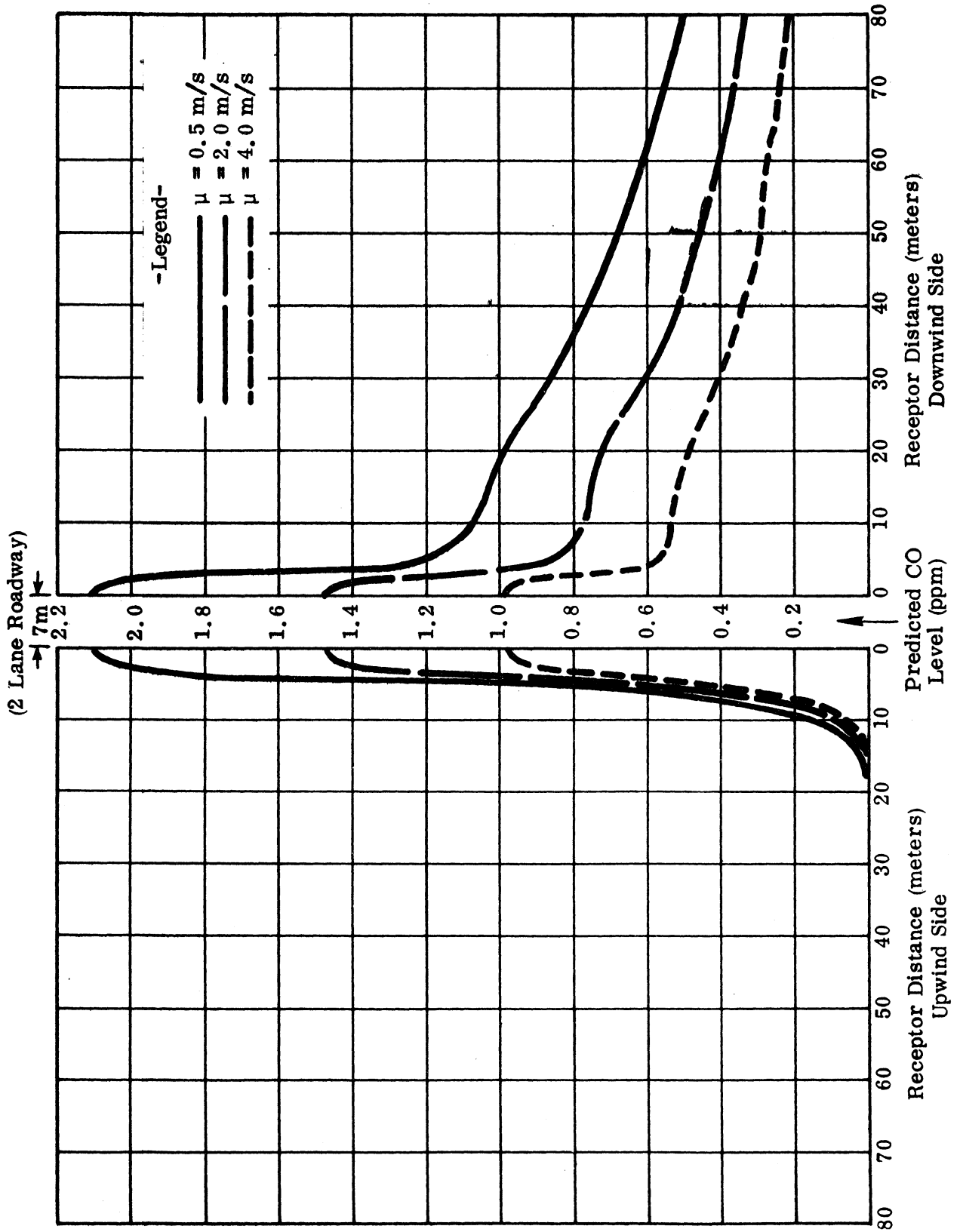
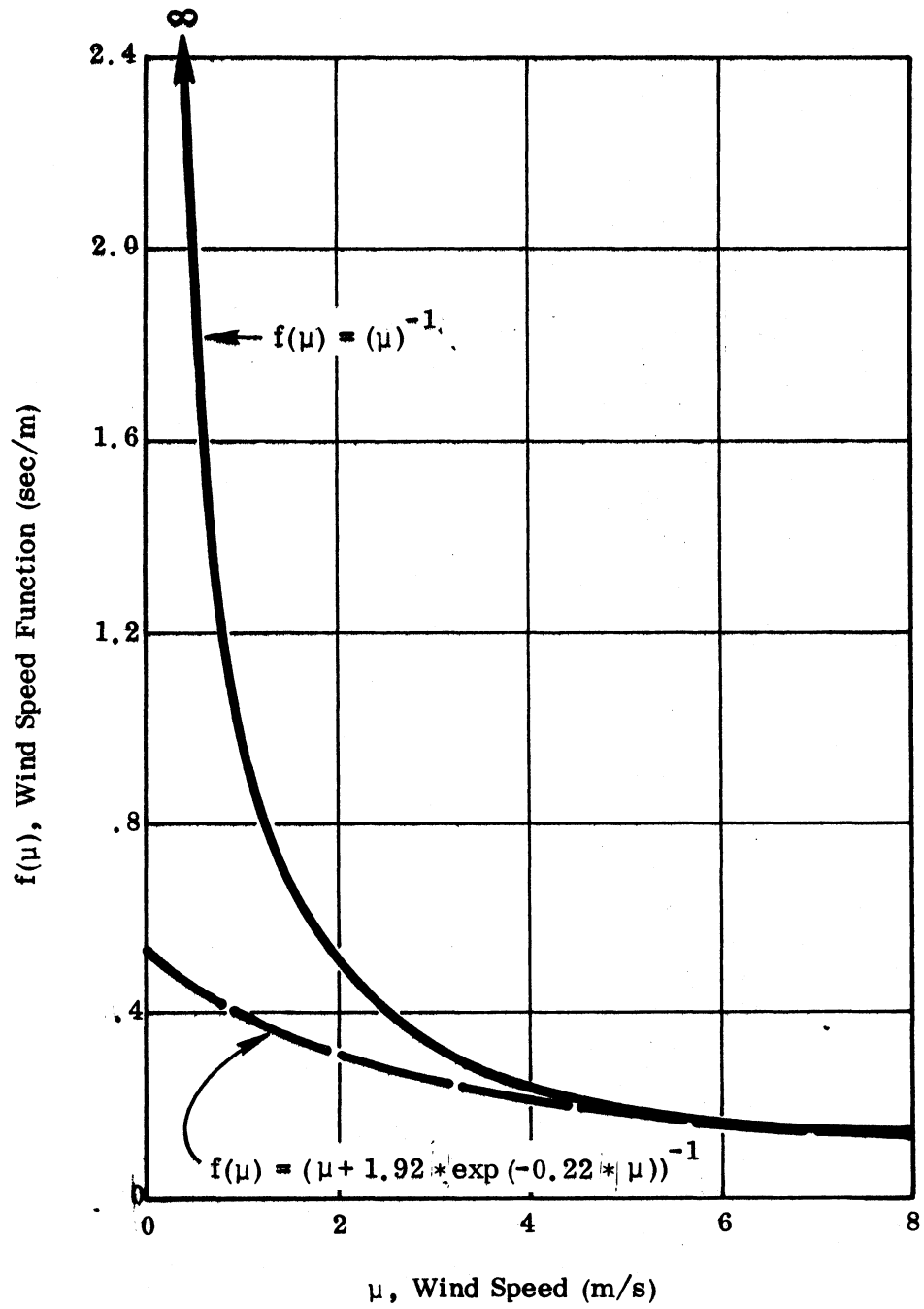Figure 5. Calculated CO concentration profiles as a function of μ, wind speed.

∞

2.4

2.0

f(μ), Wind Speed Function (sec/m)

1.6

$\leftarrow$ f(μ) = (μ)$^{-1}$

1.2

.8

.4

f(μ) = (μ + 1.92 * exp (−0.22 * μ))$^{-1}$
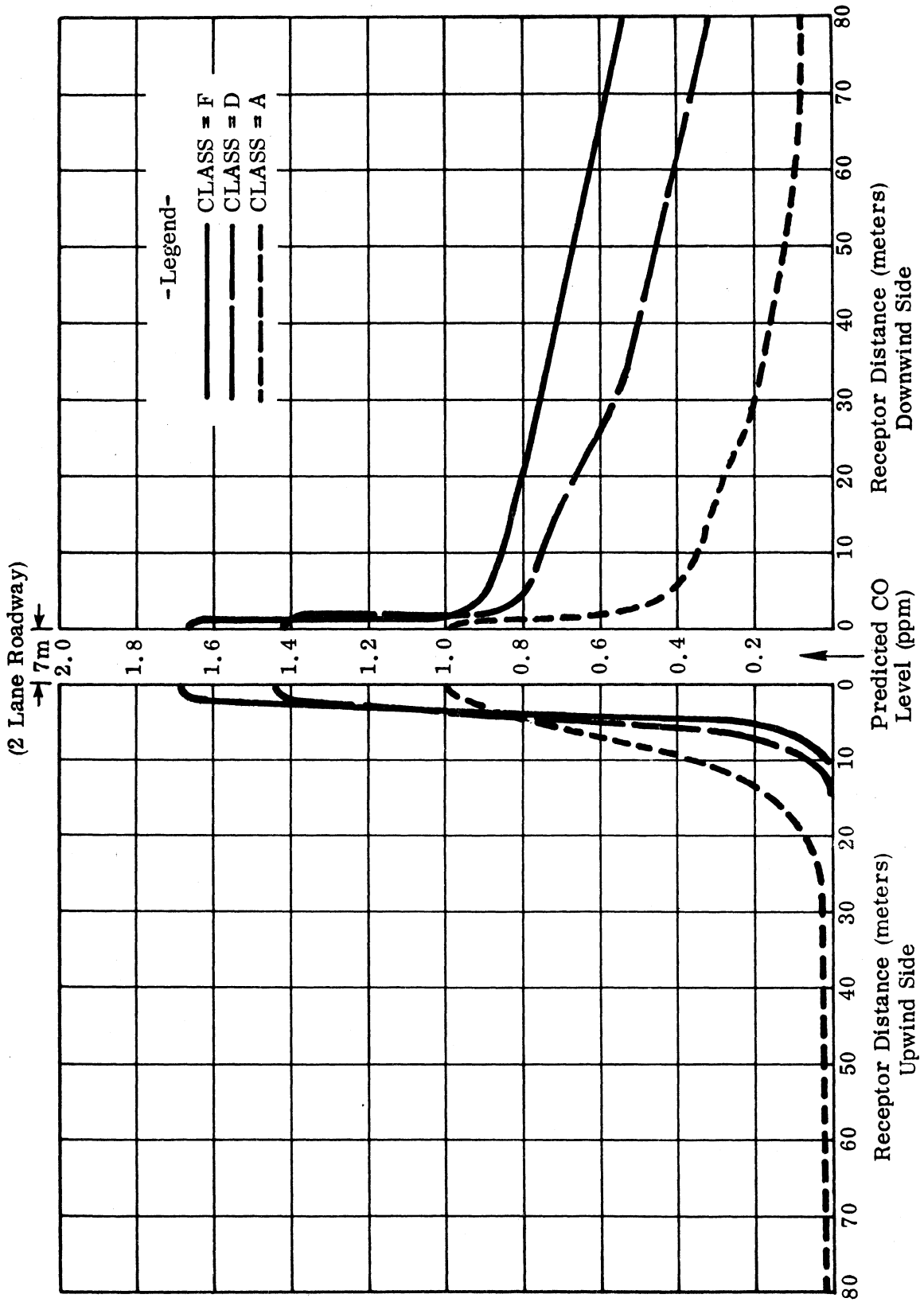
0   2   4   6   8

μ, Wind Speed (m/s)

Figure 6. f(μ) vs. μ.

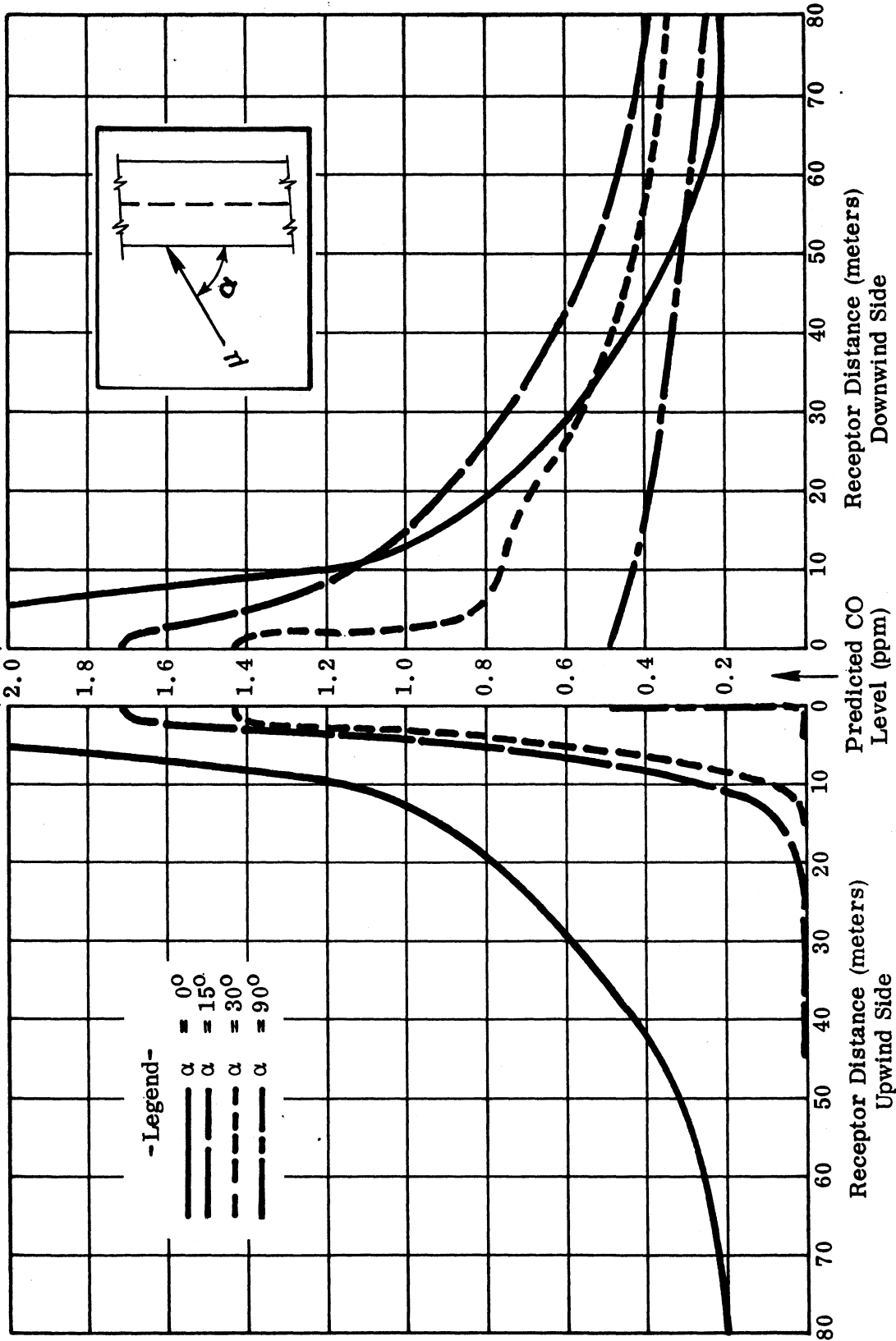Figure 7. Calculated CO concentration profiles as a function of CLASS, atmospheric stability class.

Figure 8. Calculated CO concentration profiles as a function of α, the acute angle between the road and the wind direction.
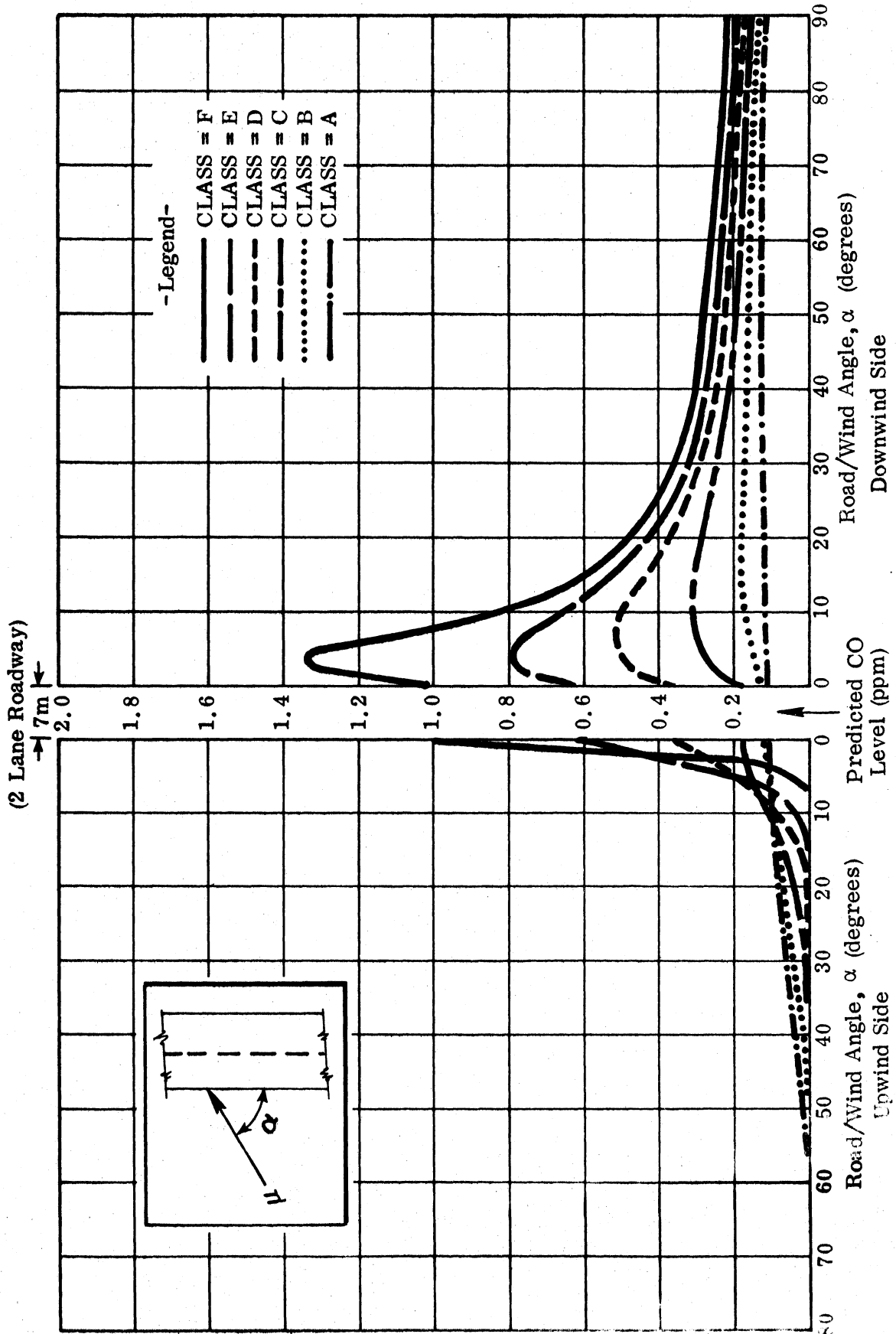
Figure 9. CO levels at receptors 15 meters from roadway vs. α as a function of CLASS, stability class.

Sensitivity to Source Emission Rate Parameters

AIRPOL-4 uses four emission rate parameters: traffic volume, average traffic speed, average traffic mix, and prediction year. The effects of these variables on CO concentrations are displayed in Figures 10 through 17.

Figure 10 illustrates the change in CO concentration profiles with variations in TFVOL, traffic volume. This change is a linear function of g_1 (TFVOL), which as Figure 11 demonstrates, is itself a linear function of TFVOL. Thus CO concentration is a linear function of the independent variable TFVOL.

Figure 12 illustrates the effect on CO concentration profiles of changes in mean traffic speed, TFSPD. This effect is a linear function of g_2 (TFSPD), which as Figure 13 illustrates, is a simple linear function of TFSPD. Therefore, CO concentration is a linear function of the independent variable, TFSPD. (This, of course, requires that TFVOL be given in veh/km.)

Figure 14 displays the variation in CO concentration profiles with changes in TFMIX, the average percentage of heavy duty vehicles. Notice that this variation is a linear function of g_3 (TFMIX, $\cdot$), as indicated by equation 33. Figure 15 illustrates the behavior of g_3 (TFMIX, $\cdot$) as a function of the mutually interdependent variables TFMIX and prediction year, notice that g_3 (TFMIX, $\cdot$) is a linear function of TFMIX. Thus for any fixed value of the prediction, year, YR, CO concentration is a linear function of TFMIX.

Figure 16 shows the variation in CO profiles with changes in YR. This variation, as indicated by equation 33, is a linear function of the factor g_3 ($\cdot$, YR). The actual behavior of the function g_3 ($\cdot$, YR) as a function of the mutually interdependent variables TFMIX and YR is illustrated in Figure 17. The reader should note that, as defined by reference 20, g_3 ($\cdot$, YR) becomes a function of TFMIX alone for all prediction years later than 1989.
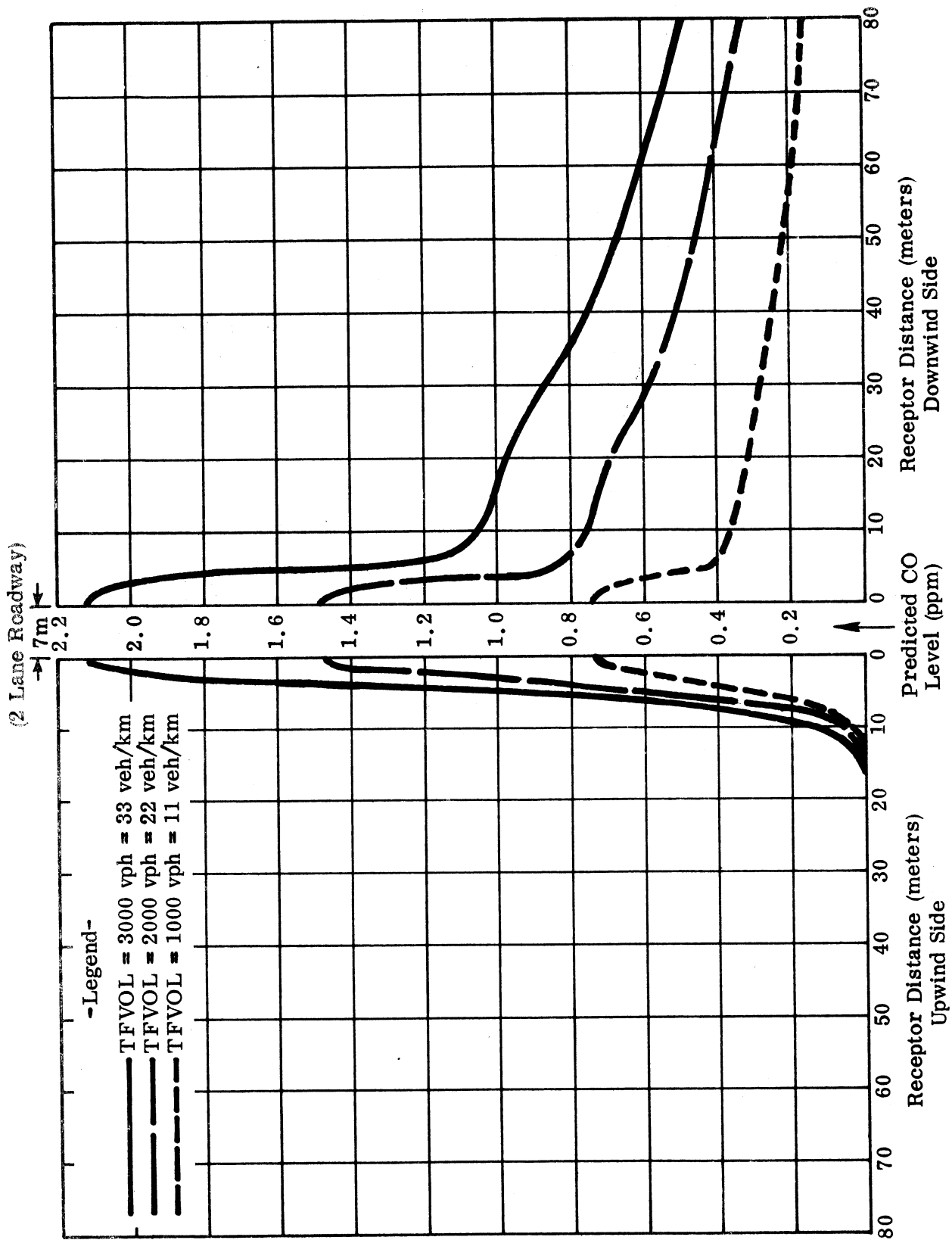
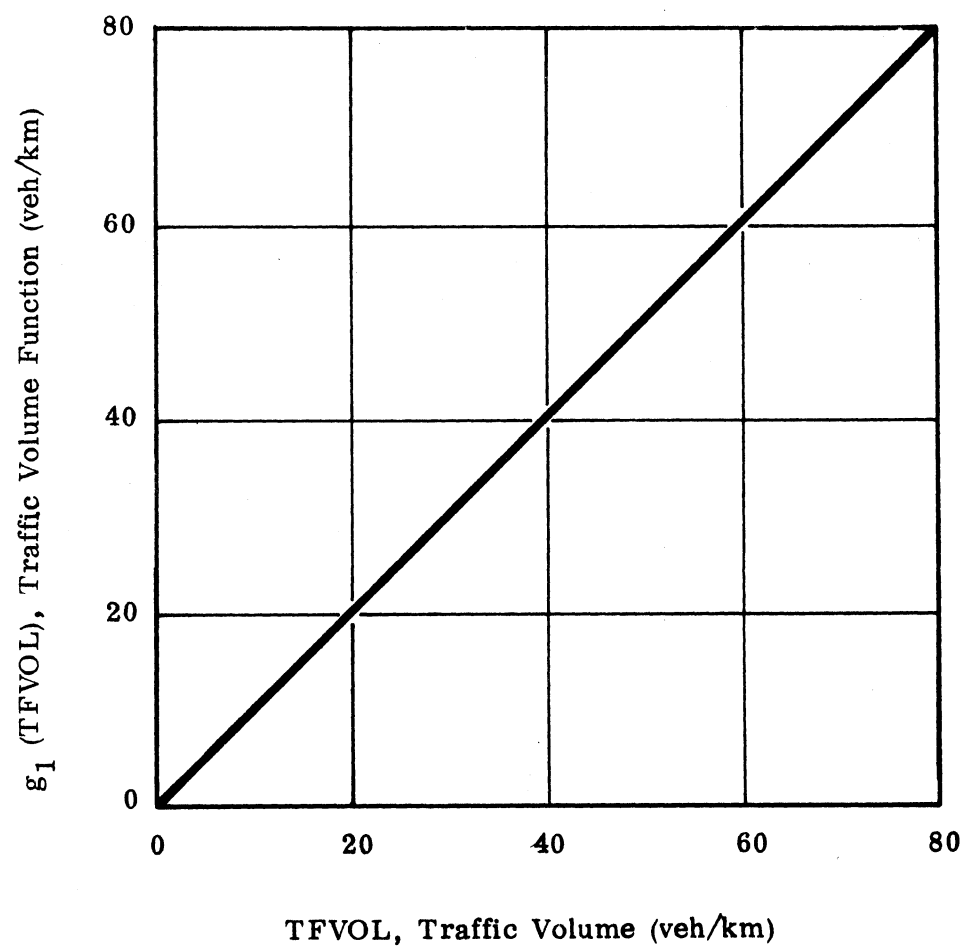Figure 10. Calculated CO concentration profiles as a function of TFVOL, traffic volume.

-Legend-

TFVOL = 3000 vph = 33 veh/km
TFVOL = 2000 vph = 22 veh/km
TFVOL = 1000 vph = 11 veh/km

(2 Lane Roadway)

Predicted CO Level (ppm)

Receptor Distance (meters) Downwind Side

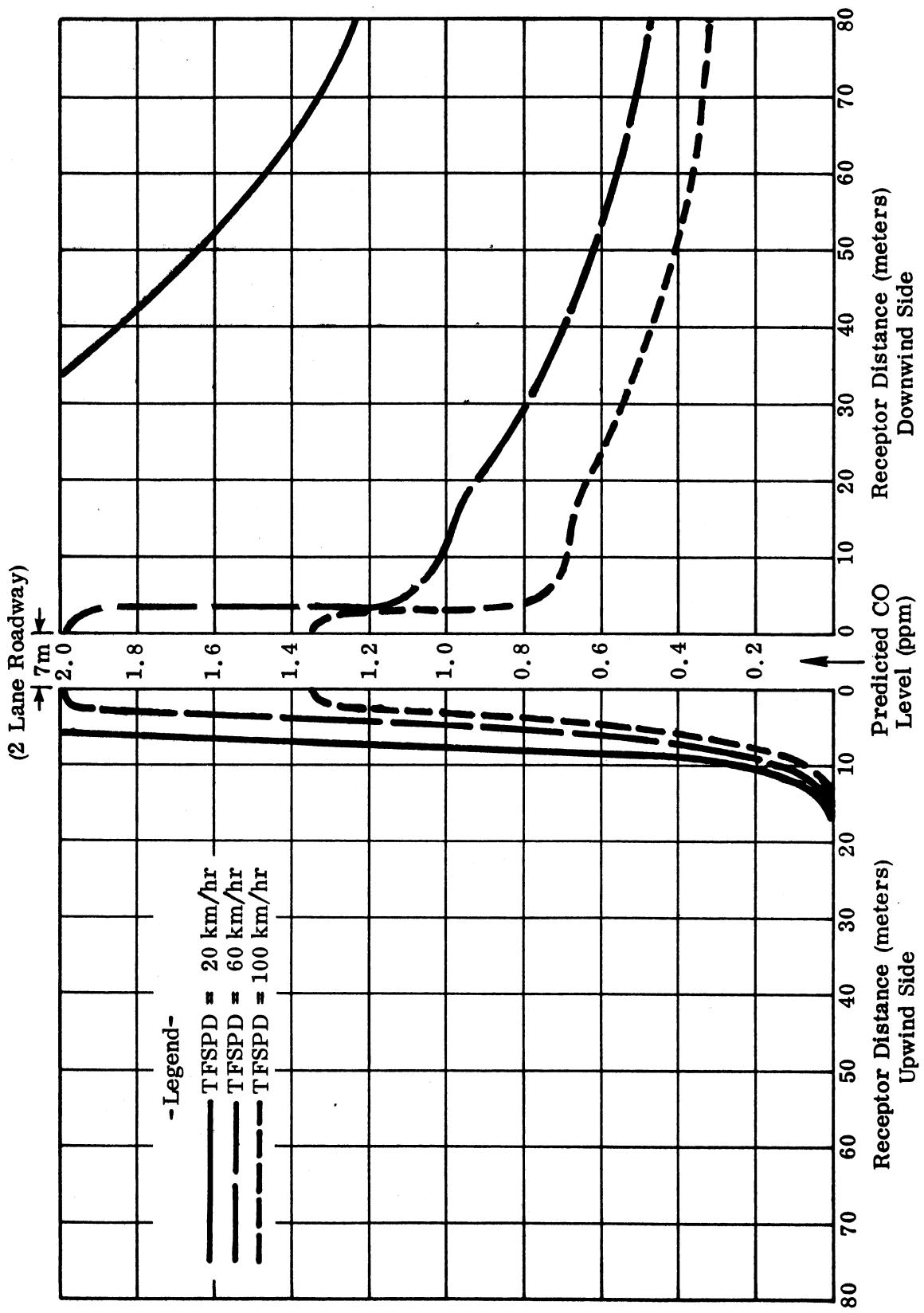Receptor Distance (meters) Upwind Side

Figure 11. g_1 (TFVOL) vs. TFVOL.

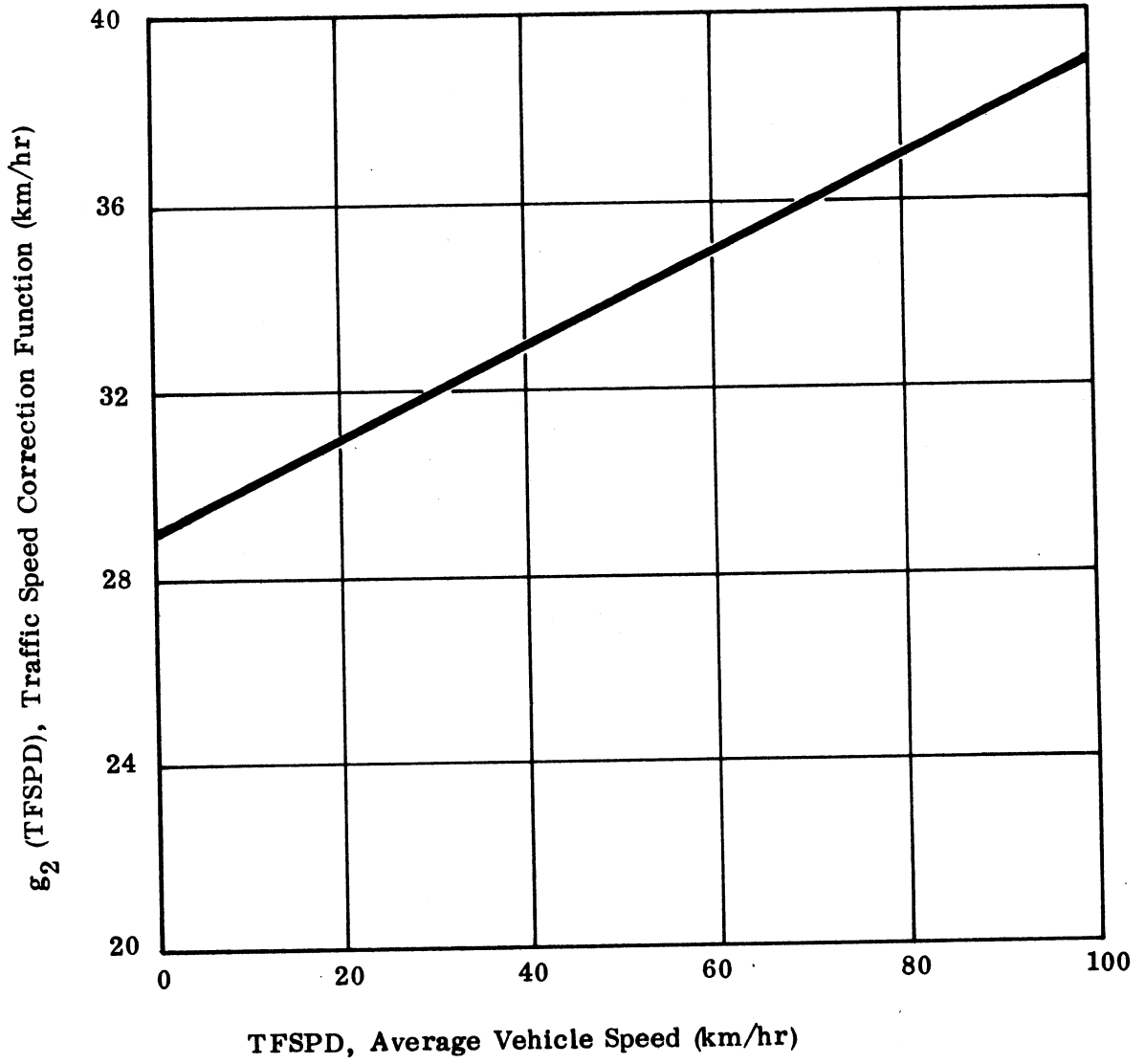Figure 12. Calculated CO concentration profiles as a function of TFSPD, mean traffic speed.
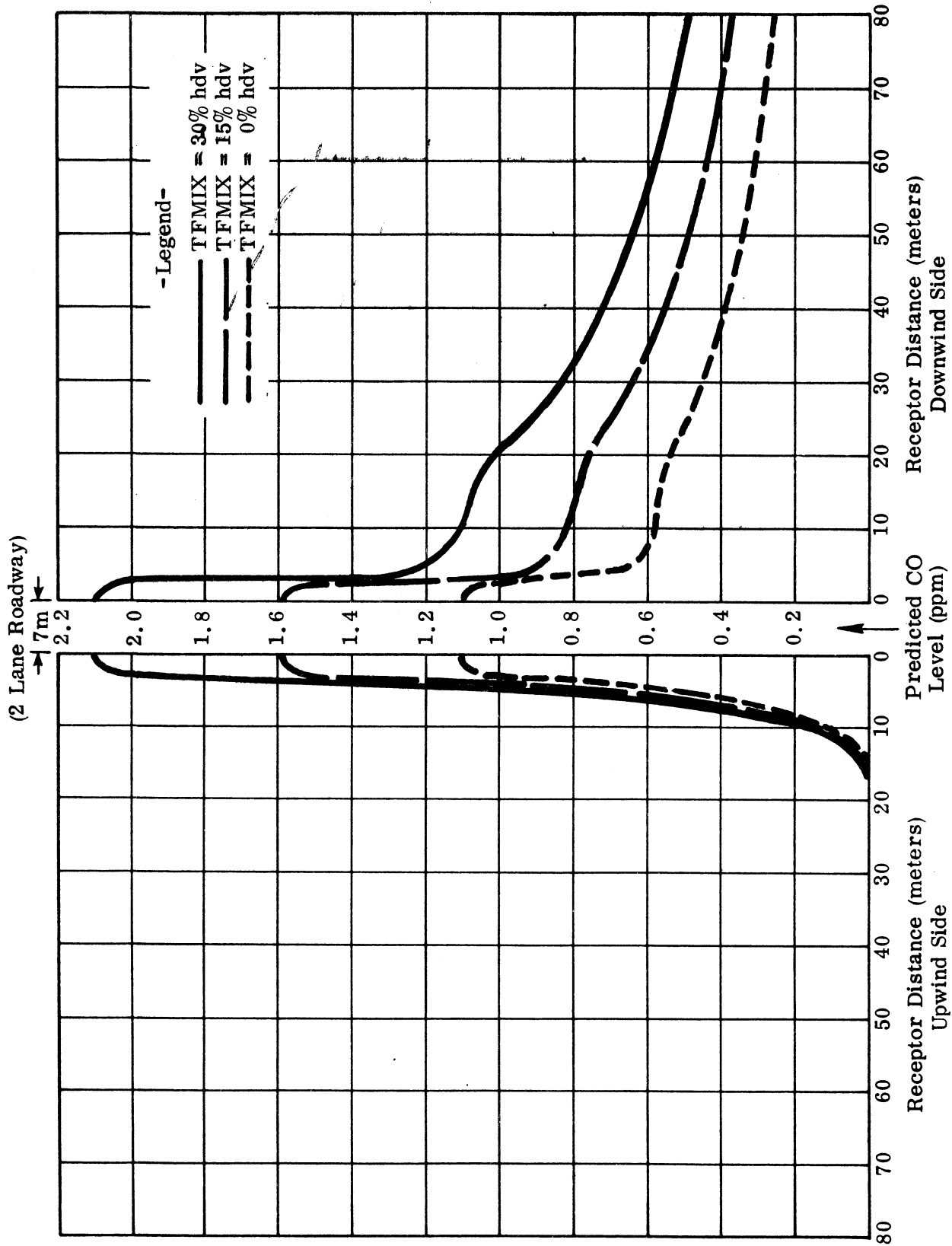
Figure 13. g_2 (TFSPD) vs. TFSPD.

Figure 14. Calculated CO concentration profiles as a function of TFMIX, traffic mix.

- 39 -
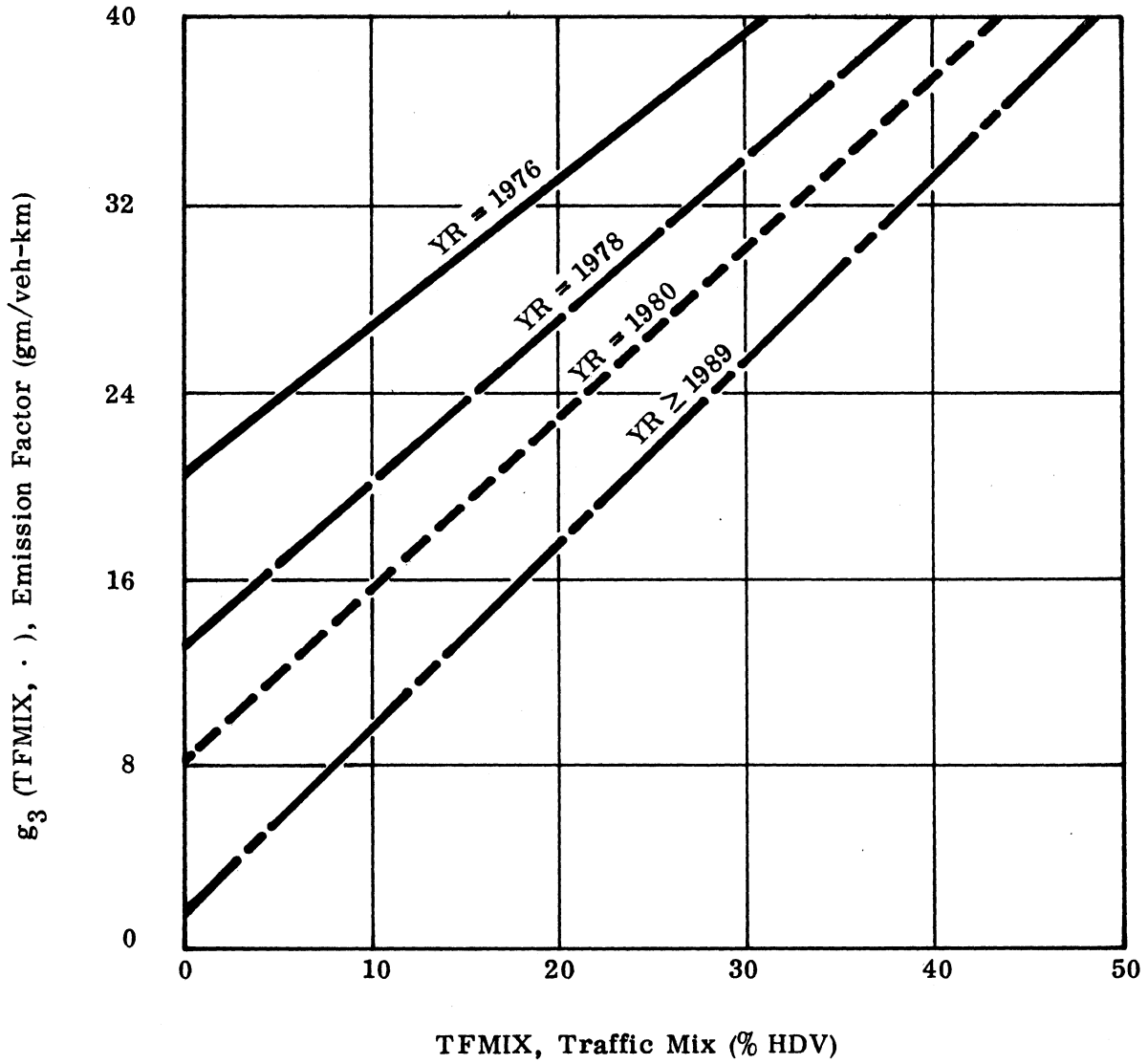
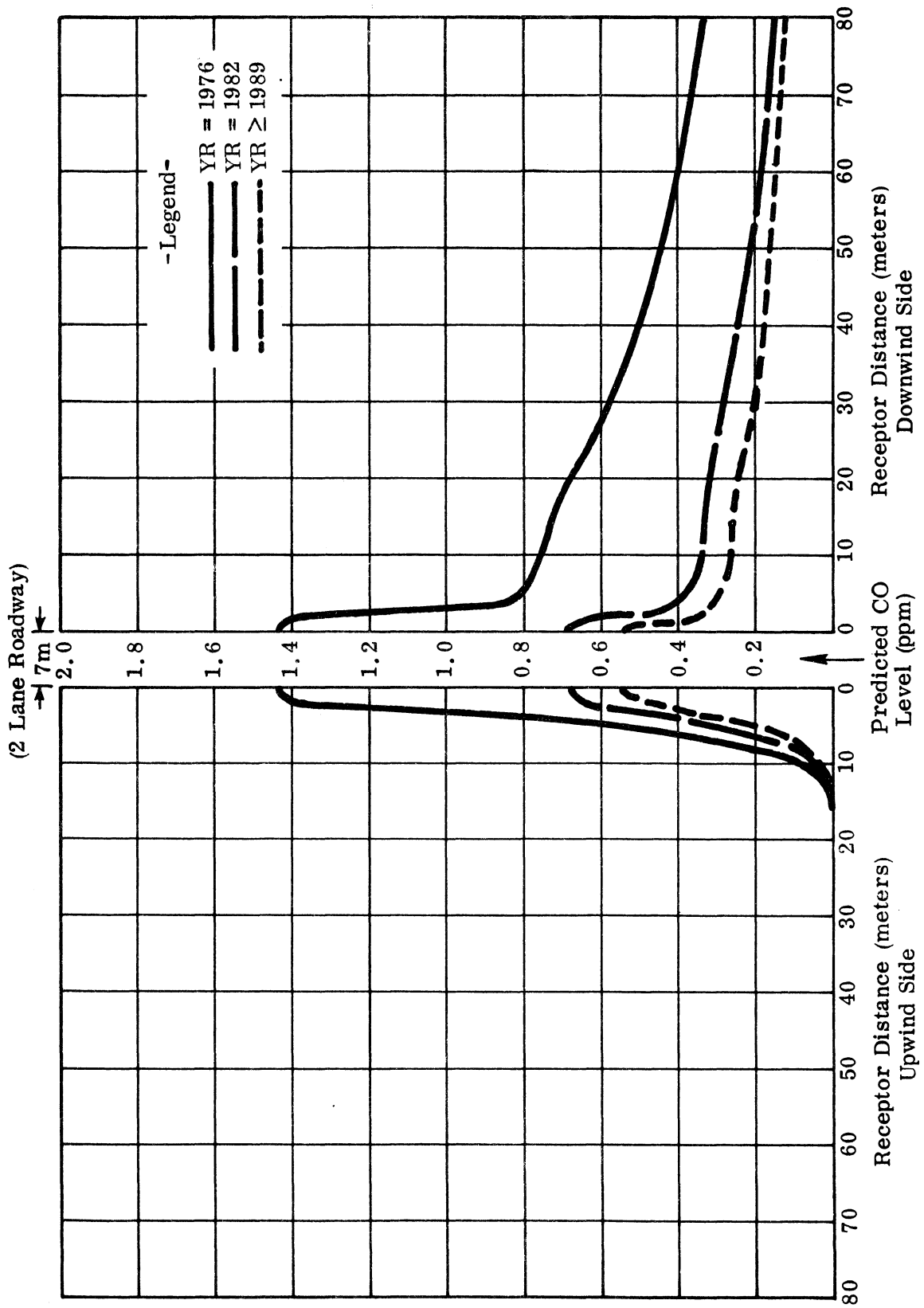Figure 15. g_3 (TFMIX, ·) vs. TFMIX as a function of YR, the prediction year.

Figure 16. Calculated CO concentration profiles as a function of YR, prediction year.
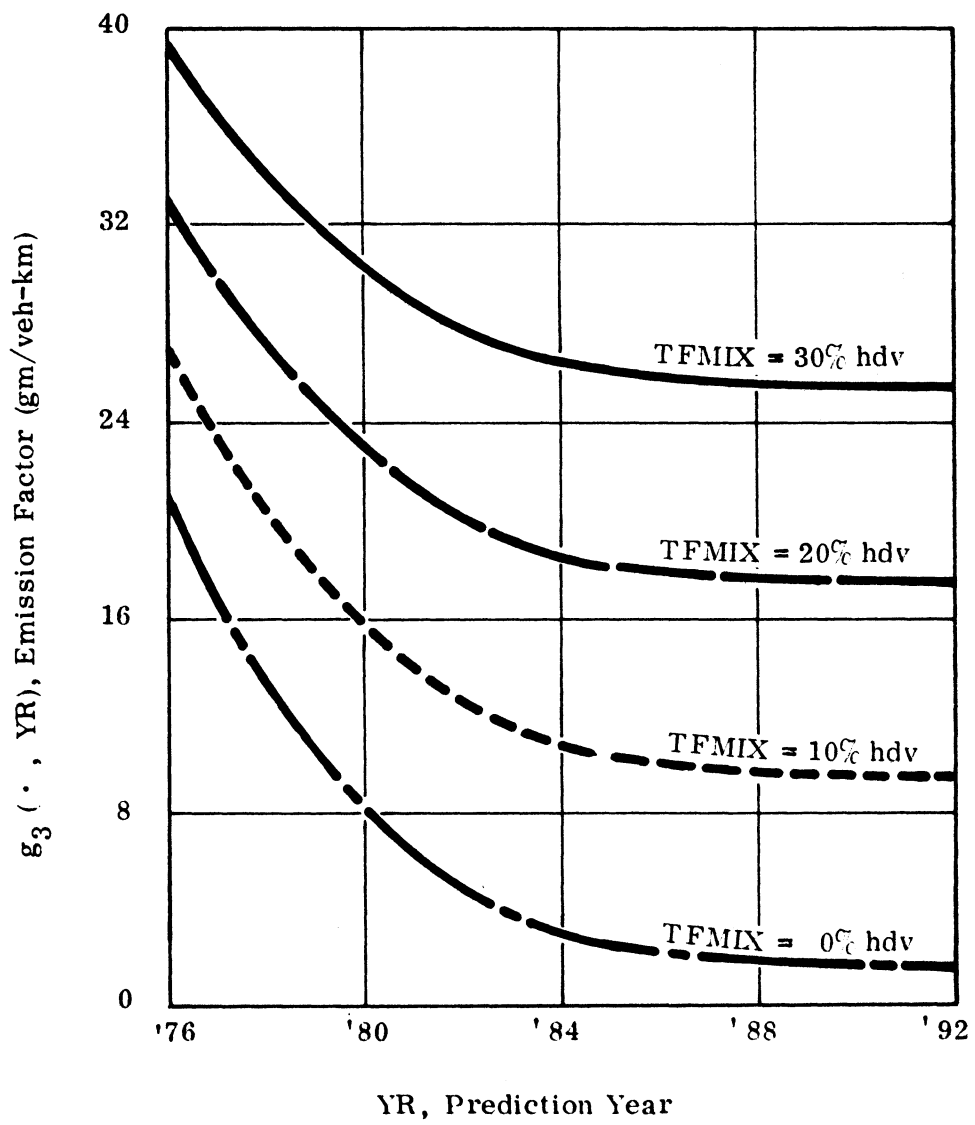
-Legend-

YR = 1976
YR = 1982
YR ≥ 1989

Predicted CO Level (ppm)

(2 Lane Roadway)
7m

Receptor Distance (meters) Downwind Side

Receptor Distance (meters) Upwind Side

Figure 17. g_3 ($\cdot$, YR) vs. YR as a function of TFMIX, traffic mix.

Sensitivity to Geometric Parameters

AIRPOL-4 considers six geometric input parameters for at grade and elevated roadways. These are source elevation, upwind source length, downwind source length, receptor elevation, receptor distance from source, and relative receptor location, i.e., whether the receptor is on the upwind or downwind side of the roadway. For roadways in cuts, AIRPOL-4 requires three additional parameters: width of the cut, length of the cut, and receptor location relative to the cut, i.e., whether the receptor is in the cut or on the plateau above the cut. The effects of these variables are considered in Figures 18 through 24.

Figure 18 shows the effect of changes in positive source elevation, SH, on CO concentration profiles. The reader should notice that concentration profiles become increasingly more sensitive to SH perturbations as SH nears zero. This is an obvious result of equations 7, 22, and 23, which demonstrate that concentration varies as a negative squared exponential of SH. Figure 18 also indicates, and these equations affirm, that concentration sensitivity to SH diminishes with increasing source to receptor distances. Furthermore, this diminution is most dramatic for small α, high atmospheric stability, and receptors upwind of a source.

Figure 19 displays the effect on concentration profiles of changes in USL, the upwind source length. As equation 7 indicates, USL will generally have a larger effect on upwind receptors than on downwind receptors. This occurs since USL is the only source of pollutants for upwind receptors; while both USL and DSL, the downwind source length, contribute to concentrations at downwind receptors. Also, the effect of USL on concentration is greatest for receptors near the source at small α. Only for a large α does USL significantly affect receptors farther than 50 meters from the source. Finally, the effect of USL is also dependent on sampling time and stability, in that high instability and long sampling times diminish the impact of USL on downwind receptors and increase its impact on upwind receptors.

Figure 20 shows the effect on CO concentration profiles of DSL, the downwind source length. For downwind receptors, this effect is most prominent at $\alpha = 90^{\circ}$ and decreases to no effect at $\alpha = 0^{\circ}$. DSL has no effect on upwind receptors under any conditions, as shown by equation 7. Also, as with all geometric parameters, the influence of DSL is a function of its mutually interdependent parameters of $h(\cdot)$.

Figure 21 illustrates the behavior of CO concentration profiles as a function of receptor elevation, RH. The reader should note that this behavior is very similar to that for SH. In fact, in a basic Gaussian formulation, the effects of SH and RH are exactly identical, as equation 7 illustrates. In AIRPOL-4, however, the influence of SH has been modified by equations 22 and 23 to reflect the increase in turbulence produced by the physical presence of a fill.

The reader should notice that concentration profiles are most sensitive to RH variations when RH is near zero. This can also be seen from equation 7, which reveals this effect to be a function of a negative squared exponential of RH. Also, as indicated by Figure 21 and affirmed by equation 7, the effect of RH diminishes with increasing source to receptor distance and is a function of the remaining mutually interdependent parameters of h (·).

The effects of receptor distance from the source, D, and relative receptor location, CASE, have been tacitly considered throughout this discussion and are best understood by simply examining the sensitivity of CO concentration profiles to all other variables. In general, concentration diminishes as D increases and concentration is less for CASE = upwind than for CASE = downwind. As with all parameters of h (·), however, explicit characterizations of the effects of D and CASE are not feasible.

Figure 22 demonstrates the influence of cut depth, CHT, on CO concentration profiles for an observer outside a cut section of roadway. The reader should observe that CHT has very little influence on concentration except near the edge of the cut. Also, the effect of CHT is a diminishing function of increasing α and increasing atmospheric instability, as equations 7 and 16 demonstrate. Additionally, this effect is a complex function of the remaining mutually interdependent parameters of h (·).

The effect on CO concentration profiles of cut width, CW, for the geometric condition of a source and a receptor in a cut is illustrated in Figure 23. (Recall that for this geometry, AIRPOL-4 forces $\alpha = 0^{\circ}$.) Notice that decreasing CW increases concentration. This increase is most dramatic at small values of CW. The reader should note that the curves in Figure 23 all maintain the characteristic bell shape as indeed they should. Source points for upwind of the receptor present a uniform distribution of pollutants at the receptor, while source points close to the receptor present a Gaussian distribution at the receptor. Thus, the receptor will be subjected to the sum of these distributions, which, as indicated in Figure 23, will be essentially a Gaussian profile shifted to higher concentrations.

Figure 24 illustrates the effect of changes in cut length, CL, on concentration profiles for receptors in a cut. This effect is particularly easy to appreciate. As figure 24 and equations 7 and 17 through 21 demonstrate, increasing CL causes an increase in concentration up to a limit determined primarily by CW, CLASS and PTIME, where PTIME is the sampling interval.
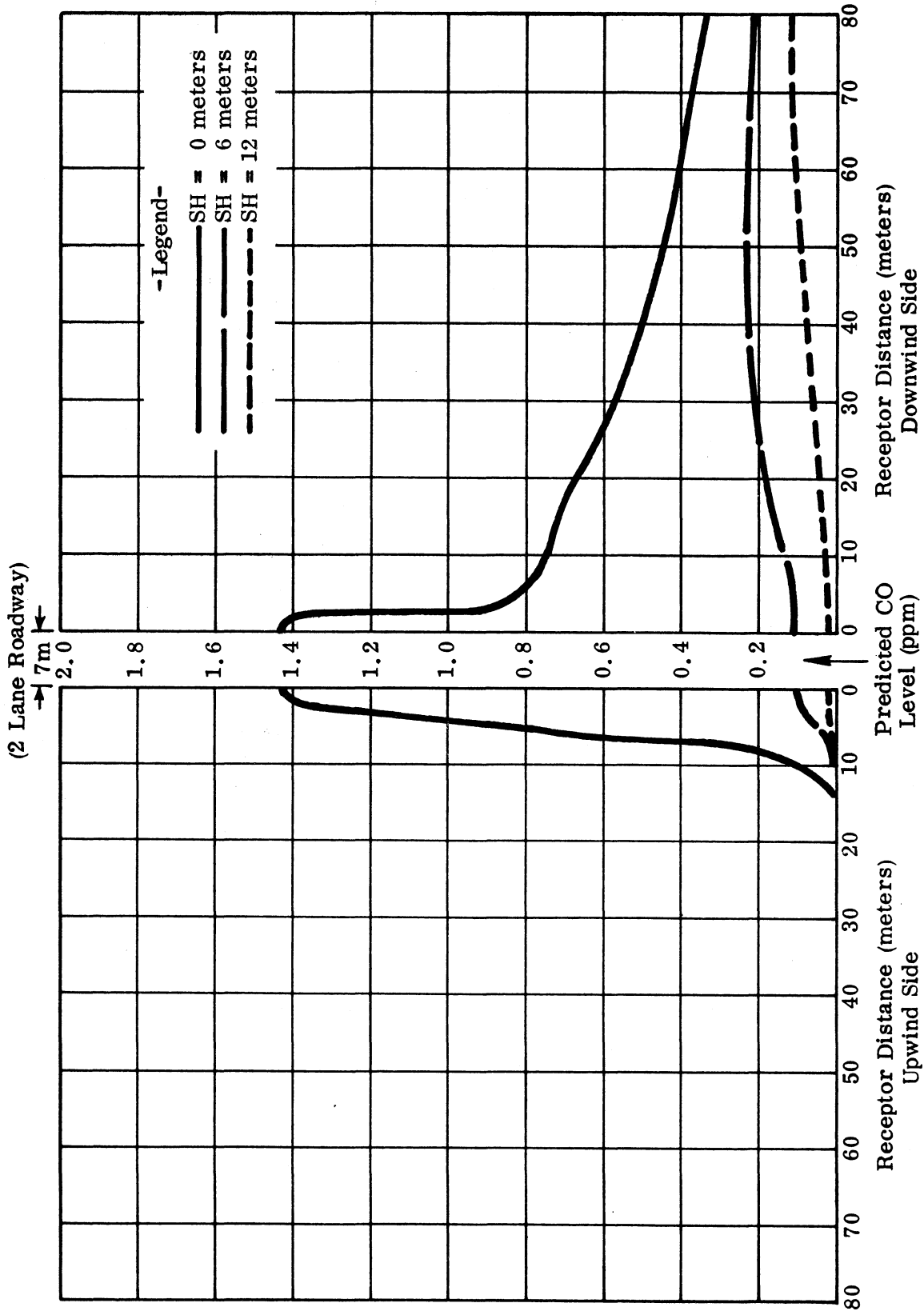
Figure 18. Calculated CO concentration profiles as a function of SH, source elevation.
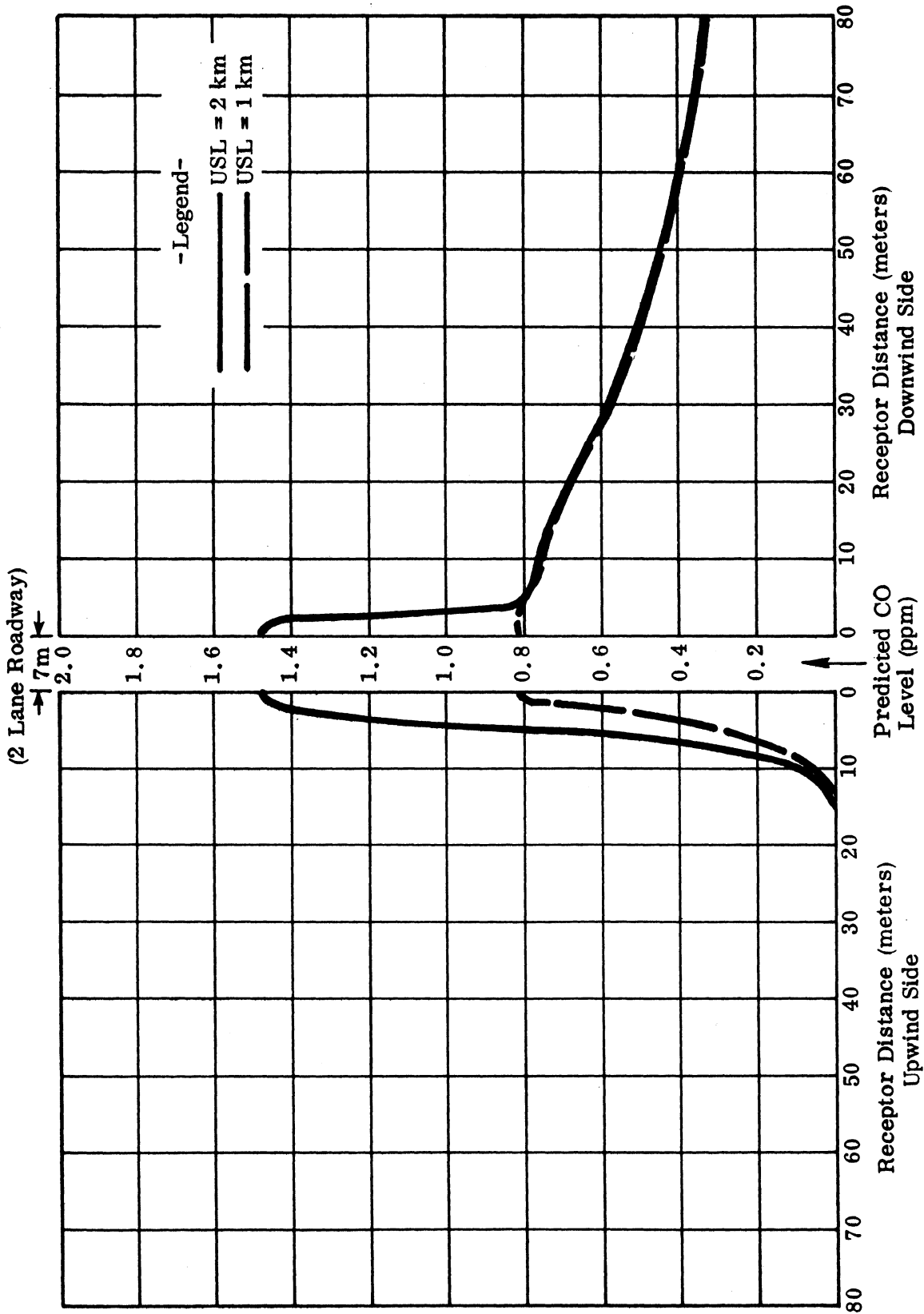
Figure 19. Calculated CO concentration profiles as a function of USL, upwind source length.
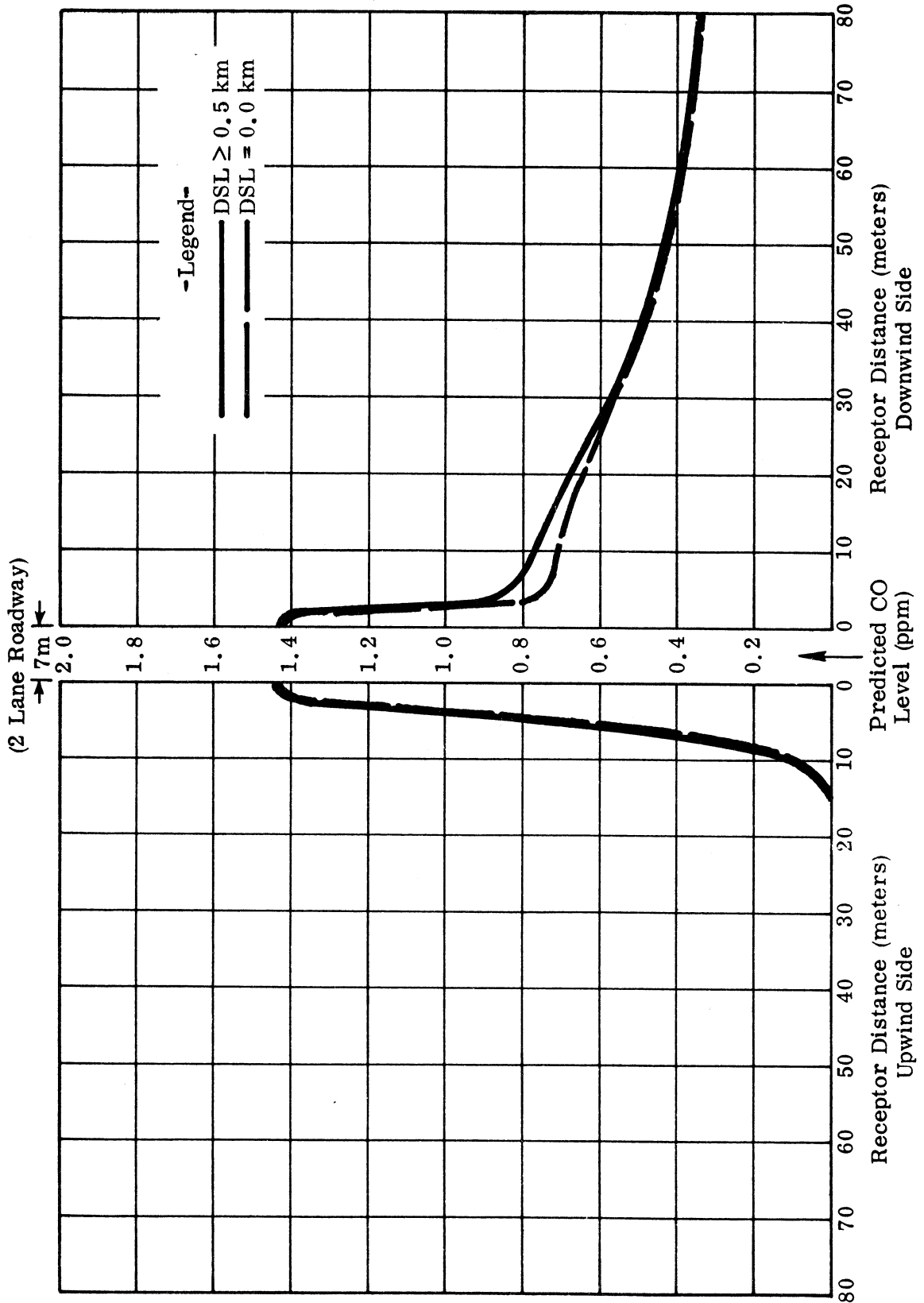
Figure 20. Calculated CO concentration profiles as a function of DSL, downwind source length.
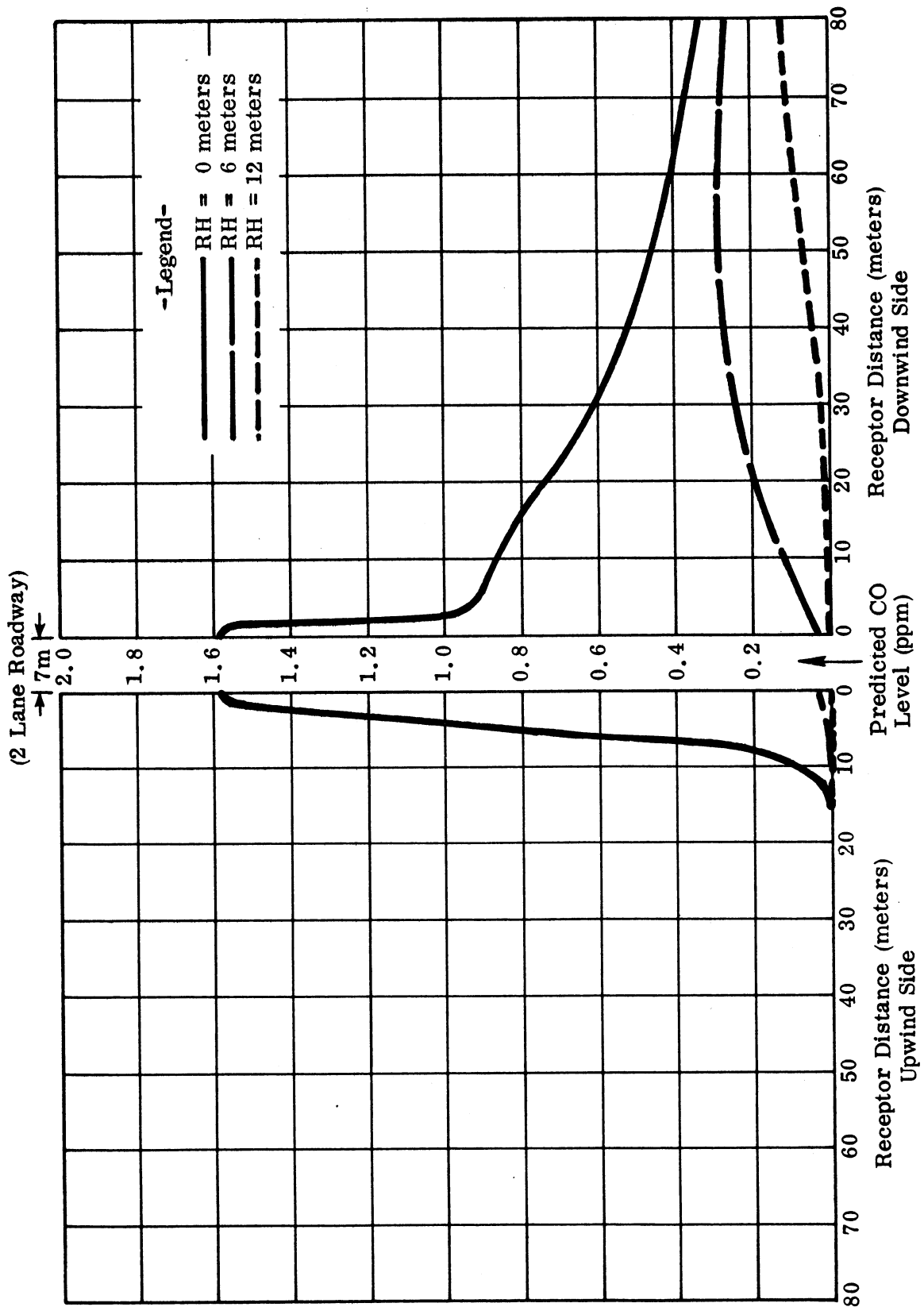
- 47 -

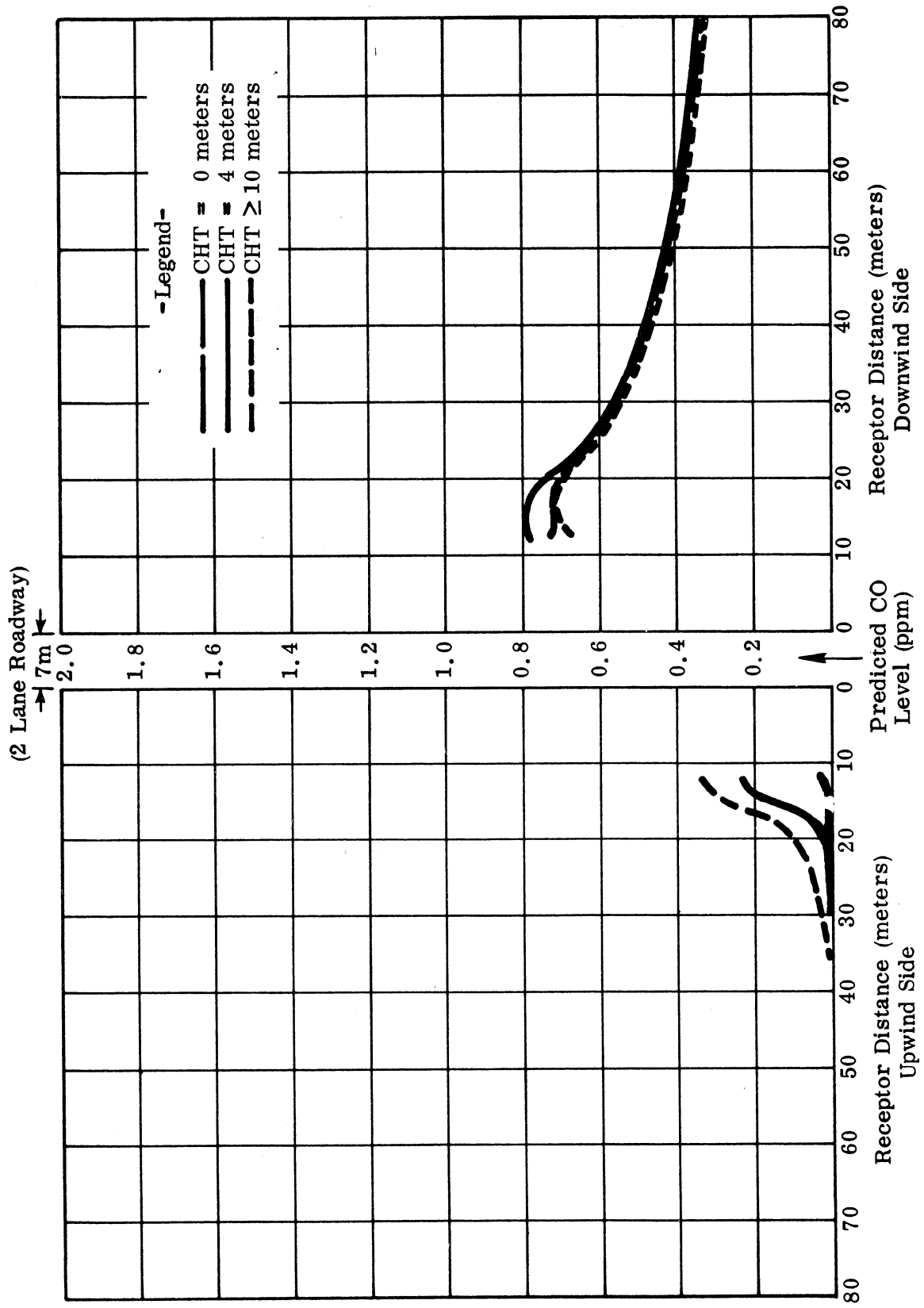Figure 21. Calculated CO concentration profiles as a function of RH, receptor elevation.

Figure 22. Calculated CO concentration profiles as a function of CHT, cut depth, for receptors outside the cut.
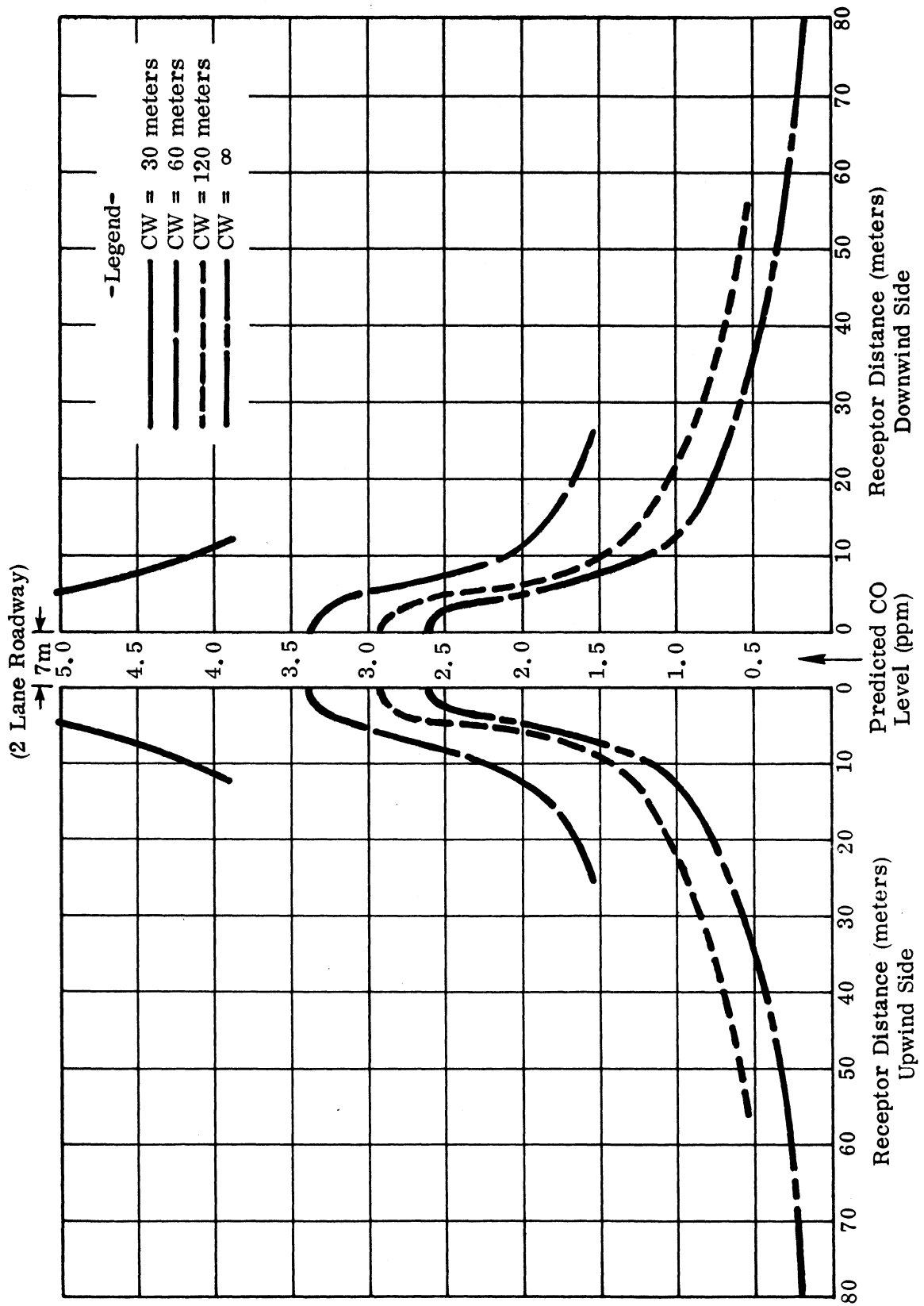
Figure 23. Calculated CO concentration profiles as a function of CW, cut width, for receptors in the cut.
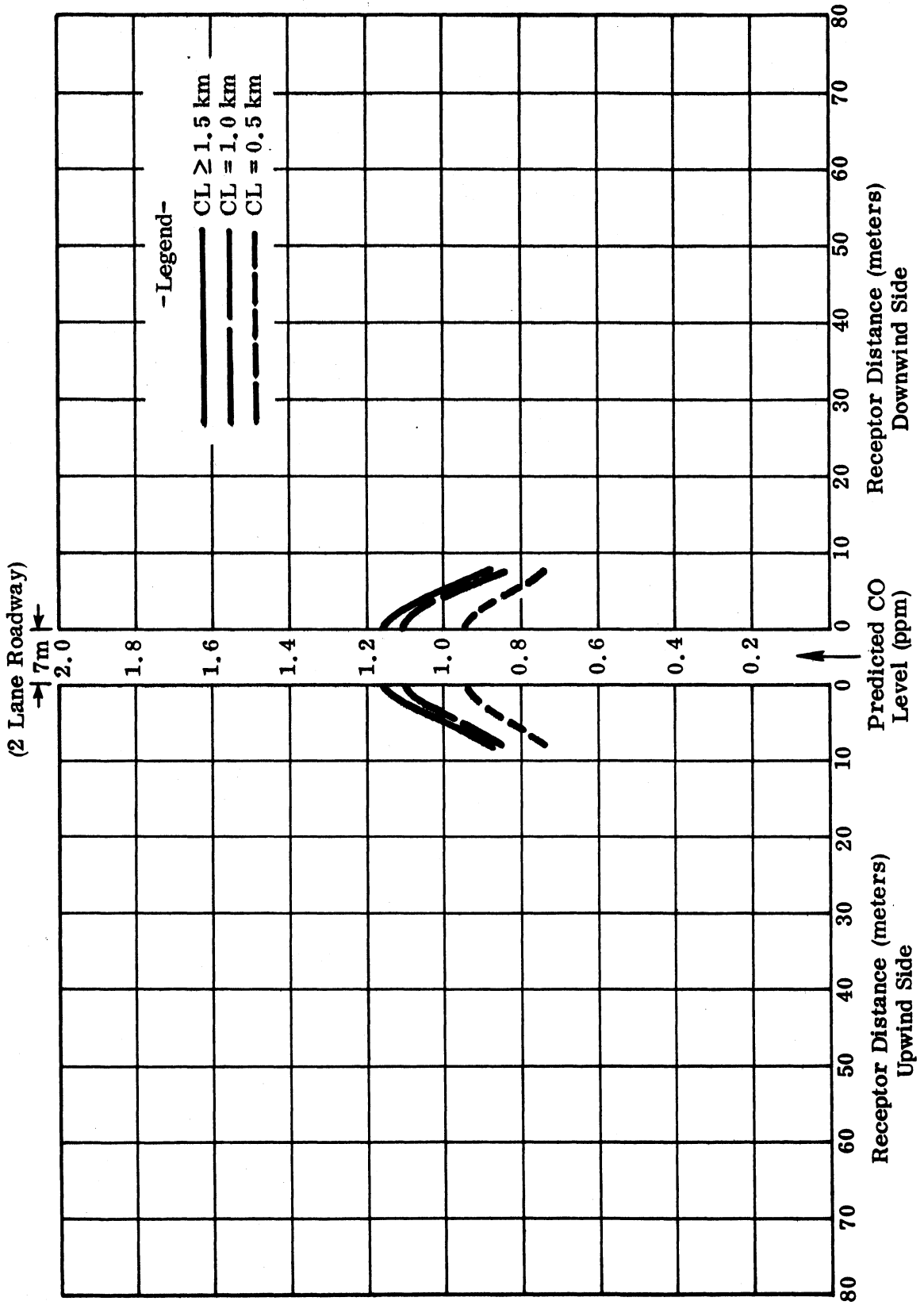
Figure 24. Calculated CO concentration profiles as a function of CL, cut length, for receptors in the cut.

Sensitivity to Sampling Time

Figure 25 illustrates the behavior of CO concentration profiles as a function of PTIME, the sampling interval. The reader should note that increasing PTIME generally results in more lateral dispersion, as indicated by equation 13. Thus, as Figure 25 demonstrates, increasing PTIME lowers peak concentrations. Notice that PTIME affects upwind receptors substantially more than downwind receptors. Also note that receptors near the source are affected more than those farther away. Furthermore, as one can deduce from equation 7, the effect of PTIME is strongest for $\alpha \approx 0^o$ and diminishes to no effect at $\alpha = 90^o$. As with the other parameters of $h(\cdot)$, the total effect of PTIME on concentration is impossible to illustrate graphically due to the mutually interdependency of these parameters.
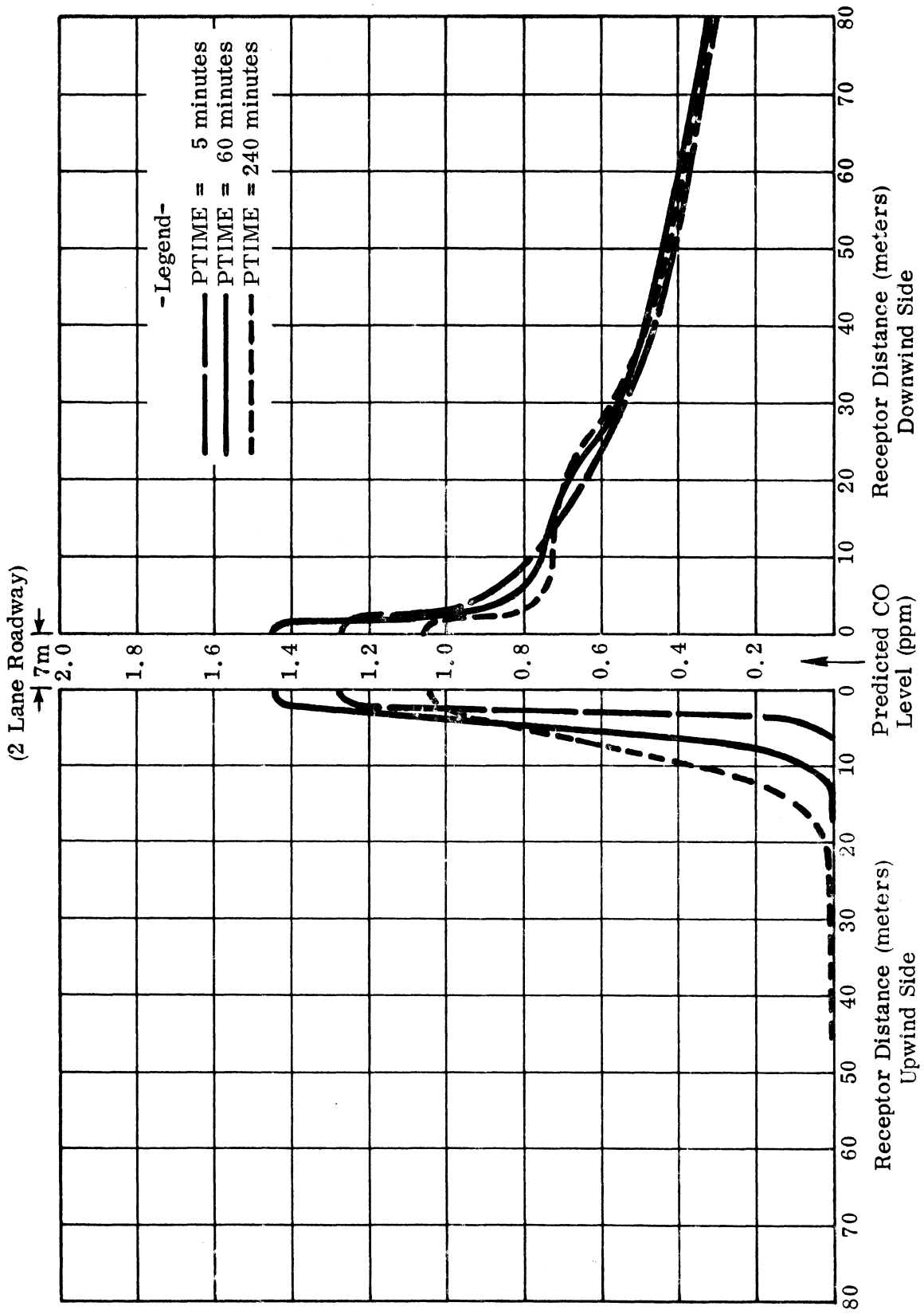
Figure 25. Calculated CO concentration profiles as a function of PTIME, sampling time.

SUMMARY

The preceding arguments have demonstrated that AIRPOL-4 is a theoretically sound extension of the basic Gaussian dispersion formulation. Furthermore, these arguments have firmly established that the innovations employed to produce AIRPOL-4 are not only theoretically valid but also mathematically tenable. Specifically, this report has demonstrated that AIRPOL-4:

1) Predicts CO concentrations upwind as well as downwind of a roadway,

2) achieves greater accuracy at a lesser cost than those Gaussian models using standard numerical integration techniques,

3) yields time averaged CO levels for any desired sampling interval,

4) predicts CO levels for urban environments,

5) transforms apparently untenable source/receptor geometries into solvable systems,

6) yields realistic (and certainly finite) predictions for all wind speeds ≥ 0, and

7) predicts CO levels for all traffic speeds ≥ 0.

RECOMMENDATIONS

This report has demonstrated that AIRPOL-4 represents a significant advancement in the field of air quality modeling in terms of both predictive theory and cost effectiveness. Thus, the Department should implement AIRPOL-4 as the predictive tool to be employed in the preparation of environmental statements.

The Department also should encourage and support research to improve the techniques for estimating atmospheric stability and the vertical and horizontal Gaussian dispersion parameters in urban environments. This research should be designed to yield a reliable method for estimating the Gaussian dispersion parameters as continuous functions of readily available meteorological and topographical variables.

REFERENCES

1. Danard, M. B., R. S. Koneru, and P. R. Slawson, 1971: A Numerical Model for Carbon Monoxide Concentrations Near a Highway, Proceedings, Symposium on Air Pollution, Turbulence and Diffusion, December 7-10, 1971, pp. 152-157.

2. Anon. 1972: Air Quality Model for Roadways, General Research Corporation Report, December 1972.

3. Wang, I. T., and D. M. Rote, 1973: A Finite Line Source Dispersion Model for Mobile Source Air Pollution, Argonne National Laboratory, Paper # 75-135.

4. Anon. 1972: Air Quality Analysis and Impact Study of Routes 85 and 87 in the San Jose Area, Aero Vironment, Inc., Pasadena, California, Report AVFR 232, November 1972.

5. Turner, D. B., 1969: Workbook of Atmospheric Dispersion Estimates, Public Health Service, Publication No. 999-AP-26.

6. Chen, T. C., and F. March, 1971: Effect of Highway Configurations on Environmental Problems — Dynamics of Highway Associated Air Pollution, Proceedings, Second International Clean Air Congress, Academic Press, 1971, pp. 35-40.

7. Beaton, J. L., A. J. Ranzieri, E. C. Shirley, and J. B. Skog, 1972: Air Quality Manual, Vol. IV: Mathematical Approach to Estimating Highway Impact on Air Quality. Department of Transportation, Report FHWA-RD-72-36.

8. Zimmerman, J. R., and R. S. Thompson, 1974: HIWAY — A Highway Air Pollution Model, Environmental Protection Agency, January 1974.

9. Anon. 1972: ESL, Inc., Report ESL-Q870, Exhibit A

10. Carpenter, W. A., 1973: A Model for Predicting Air Quality Along Highways, Virginia Highway Research Council, Report No. VHRC 73-R13, September 1973.

11. Thomas, G. B., Jr., 1960: Calculus and Analytic Geometry, 3rd edition, Addison-Wesley Publishing Co., Inc. Massachusetts, U. S. A.

12. Carpenter, W. A., G. G. Clemena, and W. R. Lunglhofer: "Introduction to AIRPOL-4, A User's Guide", Virginia Highway and Transportation Research Council, Report No. VHTRC 75-R56, May 1975.

13. Carpenter, W. A., G. G. Clemena, and W. R. Lunglhofer: Supportive Data and Methods Used for Evaluation of AIRPOL-4, Virginia Highway and Transportation Research Council, Report No. VHTRC 75-R57, May 1975.

14. Carpenter, W. A., and G. G. Clemena: Analysis and Comparative Evaluation of AIRPOL-4, Virginia Highway and Transportation Research Council, Report No. VHTRC 75-R55, May 1975.

15. Froberg, C. E., 1965: Introduction to Numerical Analysis, 2nd. edition, Addison-Wesley Publishing Co., Inc., Massachusetts, U. S. A.

16. Turner, D. B., 1964: A Diffusion Model for an Urban Area, Journal of Applied Meteorology, 3, 83-91, 1964.

17. Ludwig, F. L., A. E. Moon, W. B. Johnson, and R. L. Mancuso, 1970: A Practical, Multipurpose Urban Diffusion Model for Carbon Monoxide, Stanford Research Institute, Menlo Park, California.

18. Johnson, W. B., W. F. Dabberdt, F. L. Ludwig, and R. J. Allen, 1971: Field Study for Initial Evaluation of an Urban Diffusion Model for Carbon Monoxide, Stanford Research Institute, Menlo Park, California.

19. Environmental Protection Agency: Air Pollution Meteorology, Institute for Air Pollution Training.

20. Environmental Protection Agency, 1973: Compilation of Air Pollutant Emission Factors, Publication No. AP-42.

21. Carpenter, W. A., G. G. Clemena, W. R. Lunglhofer, AIRPOL-4 Algorithms, Virginia Highway and Transportation Research Council, Report No. VHTRC 75-R70, May 1975.